Generation of Triplet and Cation-Radical Bacteriochlorophyll *a* in Carotenoidless LH1 and LH2 Antenna Complexes from *Rhodobacter sphaeroides*†

Leenawaty Limantara,‡,⊥ Ritsuko Fujii,‡ Jian-Ping Zhang,‡ Tomisaburo Kakuno,§ Hideyuki Hara,‡ Asako Kawamori,‡ Tatsuo Yagura,‡ Richard J. Cogdell,|| and Yasushi Koyama*,‡

Faculty of Science, Kwansei Gakuin University, Uegahara, Nishinomiya 662, Japan, M&S Technosystems, 2-12-4 Mikuni-Honmachi, Yodogawa-ku, Osaka 532, Japan, and Division of Biochemistry and Molecular Biology, Institute of Biomedical and Life Sciences, University of Glasgow, Glasgow G12 8QQ, UK

Received July 27, 1998; Revised Manuscript Received October 12, 1998

ABSTRACT: The LH1 antenna complex and a native form of the LH2 complex were isolated from the carotenoidless R26 and R26.1 mutants of *Rhodobacter sphaeroides* by the use of a new detergent, sucrose monocholate. One-color, pump-and-probe transient Raman spectroscopy of these complexes using 351 nm, ∼50 ps pulses showed the generation of the triplet state of bacteriochlorophyll *a* (BChl *a*), whereas measurements using 355 nm, ∼12 ns pulses showed the generation of BChl *a* cation radical. Subpicosecond to nanosecond time-resolved absorption spectroscopy using 388 nm, 200 fs pulses for excitation showed rapid (<1 ps) generation of the triplet state and fast decay (<10 ps) of the singlet state of BChl *a*. Microsecond absorption spectroscopy confirmed the generation of BChl *a* cation radical. EPR spectroscopy using 532 nm, ∼5 ns pulses for excitation established the generation of BChl *a* cation radical. The EPR line width suggested that the unpaired electron is shared by two BChl *a* molecules. In LH1, the yield of BChl *a* cation radical per complex was estimated to be about 80% of that in the reaction center, and in LH2 about 50%. Thus, rapid generation of the triplet state, and its subsequent transformation into the cation-radical state of BChl *a* have been shown to be intrinsic properties of B870 and B850 BChl *a* assembly in the carotenoidless LH1 and LH2 antenna complexes. In the case of the carotenoid-containing LH2 complex, the triplet states of BChl *a* and carotenoid (spheroidene) were generated immediately after excitation, but the triplet-state BChl *a* was quenched efficiently by the carotenoid so that no BChl *a* cation radical was generated. Thus, the photoprotective function of the carotenoid in this antenna complex is shown.

The photosynthetic system in the membranes of purple photosynthetic bacteria consists of two different assemblies of pigment−protein complexes, that is, the light-harvesting 1 (LH1[1])−reaction center (RC) complex and the LH2 complex. The light energy captured by the LH2 complex can be transferred to the LH1 complex and eventually to the RC. The ratio of the LH2 complex versus the LH1−RC complex changes depending on the light conditions. The structures of the LH2 complexes from *Rhodopseudomonas acidophila* 10050 and *Rhodospirillum molischianum* have been determined by X-ray crystallography (*1*−*5*): It has a 9-fold or 8-fold symmetry, depending on the species, and each repeating subunit consists of a BChl pair (B850) which is aligned perpendicularly to the membrane plane and a single BChl molecule (B800) which is aligned parallel to it; the B850 bacteriochlorophyll (BChl) pair are sandwiched by a pair of peptide subunits (α and *β*) and a pair of carotenoids. Further, the structure of the LH1 complex of *Rhodospirillum rubrum* has been proposed recently on the basis of electron diffraction data (*6*): It has a 16-fold symmetry consisting of a similar repeating subunit (B890) without the B800 BChl molecule. Thus, the common structural motif of the light-harvesting complexes (LHCs) consists of the circularly stacked BChl macrocycles such as the blades of a turbine. The implication of this stacked structure has been studied extensively on theoretical bases (*7*−*11*).

To understand and appreciate the photophysical properties of the higher-order organization of the entire photosynthetic system in the light-harvesting function, we used the first strategy of examining each component. From this viewpoint, we have chosen *isolated* LH1 and LH2 complexes from

† This work has been supported by a grant-in-aid from the Ministry of Education, Science, Sports, and Culture in Japan (No. 6239101), and also by those from Human Frontier Science Program and the British Council.

* To whom correspondence should be addressed. Phone: +81-798-54-6389. Fax: +81-798-51-0914. E-mail: ykoyama@kgupyr.kwansei.ac.jp.

‡ Kwansei Gakuin University.

§ M&S Technosystems.

|| University of Glasgow.

⊥ Current Address: Faculty of Science and Mathematics, Satya Wacana Christian University, Jalan Diponegoro 52-60, Salatiga 50711, Indonesia.

[1] Abbreviations: BChl, bacteriochlorophyll; BChl $a^{+\bullet}$, bacteriochlorophyll *a* cation radical; BPhe, bacteriopheophytin; Car, carotenoid; Chl, chlorophyll; D_0, the cation-radical state; ΔH_{pp}, peak-to-peak first-derivative line width; LDAO, *N*,*N*-dimethyldodecylamine-*N*-oxide; LDS, lithium dodecyl sulfate; LHC, light-harvesting complex; LH1, light-harvesting complex 1; LH2, light-harvesting complex 2; ν_a and ν_k, the acetyl- and keto-carbonyl stretching modes; ν_r, ν_r', ν_r'', and ν_r^+, the ring-breathing (the C_a'-C_m stretching) modes in the S_0, S_1, T_1, and D_0 states, respectively; PAGE, polyacrylamide gel electrophoresis; RC, reaction center; S_0, the ground state; S_1, the lowest excited singlet state; SDS, sodium dodecyl sulfate; SMC, sucrose monocholate; T_1, the lowest triplet state; Tris buffer, 20 mM Tris-HCl (pH 8.0).

10.1021/bi981803q CCC: $15.00
Published on Web 11/21/1998

purple photosynthetic bacteria. To reveal the possible photoprotective functions of carotenoid in the LHCs, for example, quenching triplet BChl which can cause the generation of harmful singlet oxygen, and preventing the formation of cation radical which can cause oxidative degradation of BChl, we need to examine what happens in the LHCs lacking carotenoids. Therefore, we have chosen the LH1 and LH2 complexes from the carotenoidless mutants of *Rhodobacter sphaeroides* R26 and R26.1 and examined whether the triplet and the cation-radical states of BChl *a* can be generated by photoexcitation. Then, we have tried to contrast the photophysical properties of the carotenoidless LH2 complexes to those of the carotenoid-containing LH2 complex from *R. sphaeroides* 2.4.1. This comparison can be justified by the resonance Raman results suggesting that the assembly of B850 BChls and the α- and *β*-peptides in the carotenoidless LH2 complex and that in the carotenoid-containing LH2 complex are basically the same (*12*), although the former lacks carotenoid and B800 BChl. To reveal the photoprotective function, we applied high photon energy by exciting BChl *a* at Soret absorption as well as a large number of photons ($\sim 10^{15}$ photons/cm^2) which is comparable to the number of BChl *a* molecules in the beam. (The photon energy can be regarded as a physiological condition, but the number of photons must be considered to be far from the ordinary physiological conditions, although our preparation turned out to be stable enough under this extreme condition.)

A powerful technique to achieve this goal is transient resonance Raman spectroscopy: Resonance Raman spectroscopy can detect selectively a short-lived transient species whose transient absorption is in resonance with the probing wavelength; BChl *a* transient species can be detected selectively in a huge assembly of the pigment and peptides in the carotenoidless LHCs. Further, a pair of transient species with different lifetimes can be detected selectively by transient Raman spectroscopy using pulses whose durations differ by 2 orders of magnitude. It has been established previously for BChl *a* free in solution (*13*, *14*) that the frequency of the ring-breathing Raman line can identify the electronic state (whether it is the triplet or the cation-radical state, for example) and the coordination state (whether the magnesium atom is penta- or hexacoordinated). Therefore, it is now straightforward to use the ring-breathing frequency of the BChl *a* molecules bound to the LHCs to identify the electronic and coordination states induced by flash photolysis (see Figure 1a for the structure of BChl *a*). Another powerful tool is subpicosecond to microsecond time-resolved absorption spectroscopy: the electronic absorption spectra of the triplet state (*15*−*17*) and the cation-radical state (*18*) of BChl *a* have been well-established, although the spectrum of its singlet state has not been fully determined (*19*). The most powerful tool to prove the generation of the cation-radical state is EPR spectroscopy, which also provides information concerning the amount of BChl *a* cation radical generated and the extent of delocalization of the unpaired electron.

The preparation of the LH1 and LH2 complexes has been the most difficult problem to overcome before the application of resonance Raman, electronic absorption, and EPR spectroscopies to the bound BChl *a* molecules. Although the carotenoid-containing LH1 and LH2 complexes have been successfully isolated from the wild-type and a mutant of *R. sphaeroides* (*20*−*22*) and the carotenoidless "B850" LH2 complex has been isolated from the R26.1 mutant (*23*−*25*), the carotenoidless LH1 complex has never been isolated in a stable form from the tightly bound LH1−RC complex because any detergent which was strong enough to break down the LH1−RC bondage destroyed the LH1 complex itself (*25*). Further, the "B850" form of the LH2 complex turned out to be unstable following irradiation with laser pulses. Eventually, we have succeeded in the preparation of an intact LH1 complex and a stable form of the LH2 complex by the use of a combination of lithium dodecyl sulfate (LDS) and a new detergent, sucrose monocholate (SMC).

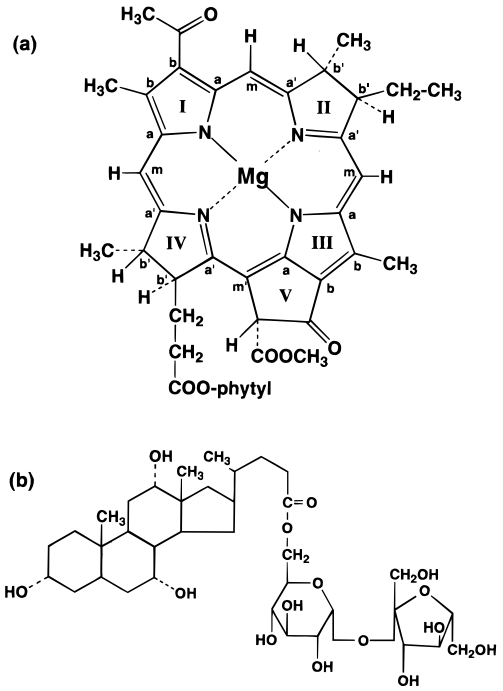

FIGURE 1: The chemical structures of (a) BChl *a* (bacteriochlorophyll *a*) and (b) SMC (sucrose monocholate).

MATERIALS AND METHODS

Chemicals. The detergent, sucrose monocholate, was a gift from Mr. Hideo Ishiwatari (it can be purchased from Dojindo Laboratories, Kumamoto, Japan); lithium dodecyl sulfate was purchased from Sigma Chemical Co. (St Louis, MO), and LDAO was purchased from Fluka Fine Chemicals (Tokyo, Japan). Chemicals used for culturing the cells and the rest of the chemicals for isolating the LHCs were obtained from Kishida Chemicals (Osaka, Japan). Chemicals used for sodium dodecyl sulfate (SDS)−polyacrylamide gel electrophoresis (PAGE) were purchased from Wako Pure Chemical Industries Ltd. (Osaka, Japan); a kit for molecular weight determination was obtained from Pharmacia Biotech (Milwaukee, WI). Bacteriochlorophyll *a* was prepared as described previously (*26*).

Culturing the Cells and Preparation of the Chromatophores. The strain of the R26 mutant of *R. sphaeroides* was a gift from Prof. R. K. Clayton and that of the R26.1 mutant was given by Prof. W. R. Sistrom. The cells were grown at 30 °C anaerobically in the succinate medium (*27*); they were irradiated through a filter 21% transparent above 500 nm (Plexiglass, GMBH Chemicals, Germany) to prevent back mutation into the wild type. The harvested cells were washed

several times with 100 mM Tris-HCl (pH 8.0) and stored in a deep freezer (−30 °C) as pellet.

The chromatophores were obtained by sonication, using an ultrasonic disruptor (TOMY UD-201, 20 kHz, 127 W), of the cells which were suspended in the above buffer to which DNase and magnesium chloride were added. The sonication was performed at 0 °C under nitrogen. The suspension was centrifuged twice at 25000*g* to remove debris. Then, the supernatant was centrifuged at 225000*g* for 90 min to pellet the chromatophores. They were washed several times to completely remove cytochromes, resuspended in 20 mM Tris-HCl buffer (pH 8.0), and stored at 4 °C. (Hereafter, 20 mM Tris-HCl buffer (pH 8.0) will be simply called "Tris buffer".)

Preparation of the LHC. The results of the preparation of the carotenoidless LH1 and LH2 complexes will be described in detail in the Results section; the carotenoid-containing LH2 complex from the wild type (2.4.1) was purified by DEAE-cellulose chromatography as descrived previously (*28*) with some modification. Only the steps in the preparation of the carotenoidless LH1 complex will be described here: (i) The R26 chromatophores ($OD_{871} = 25\ cm^{-1}$) were solubilized with 0.5% LDS at room temperature for 10 min in the dark under nitrogen. (ii) The suspension was diluted with 3 volumes of Tris buffer, and centrifuged at 25000*g* for 15 min. (iii) The supernatant was applied onto a stepwise sucrose gradient (0.75, 1.0, 1.5, and 2.0 M sucrose in Tris buffer containing 0.25% SMC; the ratio of the supernatant to the the sucrose solution is 1:4). Then, it was centrifuged at 225000*g* for 14 h. (iv) The crude LH1 (+ RC) component was collected, dialyzed against Tris buffer with 0.2% SMC, and concentrated to $OD_{871} = 25\ cm^{-1}$. (v) This component was solubilized again with 0.5% SMC at room temperature for 10 min in the dark under nitrogen. Then, the procedures (ii) and (iii) were repeated to collect the pure LH1 complex.

Preparation of the RC. The chromatophore membranes from *R. sphaeroides* R26 ($OD_{871} = 50\ cm^{-1}$) suspended in Tris buffer were under nitrogen solubilized with 0.15% LDAO in the presence of 100 mM NaCl at room temperature for 30 min in the dark. The solubilized chromatophores were centrifuged at 225000*g* for 1 h. The pellet was resuspended to the same volume of Tris buffer and solubilized again with 1% LDAO under exactly the same conditions as described above. The suspension was then centrifuged at 225000*g* for 2 h. The supernatant was a RC-enriched fraction, which was purified by DEAE-cellulose chromatography as described previously (*28*).

SDS−Polyacrylamide Gel Electrophoresis. The purified sample (LH1, LH2, or RC) was suspended into 62.5 mM Tris buffer (pH 8.0) containing 2% SDS and 1% β-mercaptoethanol (pH 6.8), and then, the suspension was heated in boiling water for 3 min. Polyacrylamide gel electrophoresis (PAGE) was performed by the method of Laemmli (*29*) using 11.5−16.5% polyacrylamide gradient gel and an Elic blot-and-slab-gel apparatus (M&S Instruments, Japan). The size of each gel-slab was 1 × 85 × 55 mm. Electrophoresis was performed for 60 min at room temperature in the constant-current mode (0.04 amps). The protein bands were then visualized by staining with 0.25% Coomassie Brilliant Blue R-250. Photographs were taken after destaining the gel with a solution containing 20% ethanol and 10% acetic acid.

Stationary-State Electronic Absorption Spectroscopy. The ground-state, electronic absorption spectra of the pigment−protein complexes and the chromatophores were recorded at room temperature by using a Hitachi U-2000 double-beam spectrophotometer.

Resonance Raman Spectroscopy. The carotenoidless LH1 and LH2 complexes were suspended in Tris buffer containing 0.2% SMC at a concentration of OD (Q_y) ≈ 100 cm^{-1}, whereas the carotenoid-containing LH2 complex was suspended in Tris buffer containing 0.1% LDAO at the same concentration. Each suspension was sealed under a nitrogen atmosphere into an ampule, which was used as a spinning cell. Two different types of light source were used: one, the 351 nm, 50 ps and 1 kHz pulses from a combination of a Nd:YLF laser (Quantronix 4216) and a Nd:YLF regenerative amplifier (Quantronix 4417); and the other, the 355 nm, 12 ns and 10 Hz pulses from a Nd:YAG laser (Lumonics HY-400). Each of the "picosecond" and "nanosecond" transient Raman spectra was obtained as a difference spectrum by subtracting the low-power spectrum (2−3 mW, defocused) from the high-power spectrum (25 mW, focused) (*30*). In the high-power measurements, the photon densities applied were approximately 1.1×10^{15} and 1.1×10^{17} photon·pulse^{-1}·cm^{-2} in the picosecond and nanosecond Raman spectroscopy, respectively. The number of photons used for excitation was on the same order as the number of molecules in the beam in the former, and the number of photons was by 2 orders of magnitude larger than the number of molecules in the latter.

The low-power spectrum was regarded as a ground-state (S_0) Raman spectrum. We will present only the S_0 Raman spectra detected by using the nanosecond pulses for the LH1, "B860" LH2, "B850" LH2, and RC complexes (see the first subsection of the Results section for the definition of "B860" and "B850" LH2 complexes) because the S_0 Raman spectra detected by using the picosecond pulses were essentially the same, but their S/N ratios were slightly lower. The picosecond and the nanosecond transient Raman spectra will be presented only for the LH1, the B860 LH2, and the RC complexes, because the B850 LH2 complex was destroyed by high-power pulsed excitation. Smoothing was performed for the transient Raman spectra by filtering Fourier transformed high-frequency components using a Haning filter.

Subpicosecond to Nanosecond Time-Resolved Absorption Spectroscopy. Each of the carotenoidless LH1 and B860 LH2 complexes and the carotenoid-containing LH2 complex were suspended in the same buffer as in the case of Raman spectroscopy at the concentration of OD (Q_y) = ∼10 cm^{-1}. Before each measurement, the suspension was deoxygenated by repeating, for 20∼30 cycles, gentle vacuuming and subsequent filling with high-purity nitrogen gas. A peristaltic pump was used to circulate the suspension through a flow-cell (optical path, 1 mm) from and to a sample reservoir (15−20 mL) which was cooled in an ice−water mixture. The sample suspension was purged with the nitrogen gas during the measurement. A 5.0×10^{-5} M BChl *a* solution of pyridine was also examined.

The setup for time-resolved absorption spectroscopy was as follows: The output pulses (776 nm, 120 fs, 1 kHz, and 1 mJ/pulse) from a regenerative amplifier (Spectra Physics, Spitfire) which was seeded by a mode-locked Ti:sapphire laser (Spectra Physics, Tsunami) was split into two compo-

nents by using a 10% thin-film beam splitter. The major component was frequency-doubled by the use of a type I BBO crystal (0.5 mm thick) to generate the pumping pulses at 388 nm, and the minor component was focused into a water cell (10 mm thick) to generate a white continuum. The white continuum was split by the use of a 50% broad-band beam splitter into the probe and the reference beams; the former was overlapped with the pumping beam with an angle of 5−7°. The polarization of the probe beam was set to 54.7° with respect to the vertically polarized pump beam. The probe and reference beams were focused onto the upper and lower parts of the entrance slit of a spectrometer (Spex 270 M) equipped with a two-dimensional CCD detector (Princeton Instruments, LN/CCD 1152 EUV). The delay time between the pump and probe pulses was controlled by a computerized optical delay line. For each measurement, the nonresonant optical Kerr effect signal of the buffer or the solvent was measured and used for the correction of the group velocity dispersion (*31*). The full-width-at-half-maximum of the cross-correlation traces between the pump and probe pulses was determined by the optical Kerr effect signal to be about 220 fs as an average for all of the wavelength region. For the measurement of the region above 700 nm, a glass filter (HOYA O-560) was set in front of the entrance slit to avoid second-order interference; a pair of spectra were then combined to cover the 400−950 nm region. The photon density applied to the sample was 6.9×10^{15} photon·cm^{-2}, and the number of photons and the number of molecules in the beam were comparable. No smoothing of the observed spectra was performed.

Submicrosecond to Microsecond Time-Resolved Absorption Spectroscopy. The concentrations of the carotenoidless LH1 and LH2 complexes and the carotenoid-containing LH2 complex were adjusted to OD (Q_y) = 6 cm^{-1}. Before each measurement, the suspension in a cubic quartz cell (optical path, 2 mm) was deoxygenated by bubbling nitrogen gas through it; it was kept under the nitrogen atmosphere during the measurement. The solutions of BChl *a* dissolved in pyridine and carbon tetrachloride (3×10^{-4} M) were also measured for comparison. The pumping pulses (355 nm, 12 ns, 1 Hz, and 15 mJ/pulse) were obtained as the TH from a Nd:YAG laser (Lumonics, HY-400). The probing pulses (60 μs) which were obtained from a Xe flash lamp (Tokyo Instruments, XF-80) were split by a 50% beam splitter into the probe and the reference beams; the pump beam crossed the probe beam on the sample cell with an angle of ∼20°. The probe and the reference beams were focused, through an optical fiber lens system, onto the entrance slit of a spectrometer (Acton, SpectraPro 275i) which was equipped with a dual intensified diode array detector (Princeton Instruments, DIDA-512 GR). The timing among the pumping and the probing laser pulses and the gating pulse (50 ns) for the detector was controlled electronically by using a combination of a digital delay pulse generator (Stanford Research Systems DG535) and a high-voltage pulse generator (Princeton Instruments, PG-200). The photon density applied to the sample was 8.5×10^{17} photon·pulse^{-1}·cm^{-2}, and the number of photons exceeded by 2 orders of magnitude the number of molecules in the beam.

EPR Spectroscopy. Each sample in suspension or in solution ($OD_{max} \approx 100$ cm^{-1}) was loaded into a Suprasil quartz tube (inner diameter, ∼ 4 mm) and stored in liquid nitrogen until EPR measurement. Transient EPR spectra were recorded by using a Bruker ESP 300E system equipped with a transient microwave bridge (ER 046XK-T). The sample was irradiated through a window (diameter, 6 mm) of a TE_{011}-mode cylindrical cavity with the 532 nm pulses (power, 50 mJ; duration, 5 ns; and repetition, 1 Hz) from a Nd:YAG laser (Continuum, Surelite I). A capillary containing Cr^{3+}-doped MgO ($g = 1.9800$) was set inside the cavity as a reference to calibrate g values and intensities. To improve the S/N ratio, 100 kHz magnetic field modulation with an amplitude of 3 G was applied, and the EPR signal was detected by using a lock-in amplifier with a time constant of 200 μs. The timing between the laser pulse and the transient EPR measurement was adjusted by a digital delay pulse generator (Stanford Research Systems DG 535) which was controlled by a personal computer (IBM Aptiva 730). External triggers were applied to start recording 200 μs earlier than the laser flash excitation. A set of 20−40 transient signals was accumulated. Temperature was set to 110 or 250 K by the use of a continuous-flow He cryostat (Oxford ESR-900).

In chemical oxidation experiments, ∼50 mM potassium ferricyanide was added to the suspension of the LH1 complex in Tris buffer ($OD_{873} = 100$ cm^{-1}) containing 0.2% SMC. CW EPR spectra were recorded at 110 or 296 K by a conventional method within 5 min after the addition of ferricyanide.

Table 1: Characteristics of the Cultures of *Rhodobacter sphaeroides* R26 and R26.1

parameter	R26	R26.1
growth rate	slow	fast
suspension	pinky blue	blue
supernatant	pink	pale yellow
sediment	blusih grey (well-packed pellet)	blue (loose sediment)
Q_y absorption	873 nm	863 nm

RESULTS

Isolation and Characterization of the Carotenoidless LHCs from R. sphaeroides. Since the R26 mutant contains only the LH1 complex (*25*, *32*, *33*) and the R26.1 mutant contains both the LH1 and LH2 complexes (*25*), the LH1 and the LH2 complexes were isolated from the R26 and R26.1 mutants, respectively. Table 1 lists the characteristics of the two mutants: They are different in growth rate, and in the colors of culture, supernatant, and cells. The wavelength of the Q_y absorption is useful to distinguish the two mutants.

Sucrose monocholate (SMC, see Figure 1b for the structure) is a nonionic derivative of cholic acid. Due to the addition of the sucrose group, it becomes less hydrophobic than cholic acid. Since both moieties of steroid and carbohydrate have plane structures, the detergent can cover the surface of a membrane protein without destroying its three-dimensional structure. Therefore, at an appropriate concentration, this detergent would not disturb significantly the pigment−protein and pigment−pitment interactions. SMC has a cmc value of 4.7 mM, and therefore, it can be easily removed by dialysis under the concentrations below 5 mM. Since solubilization of the LHCs using this detergent alone was found to be not efficient enough, we decided to use both

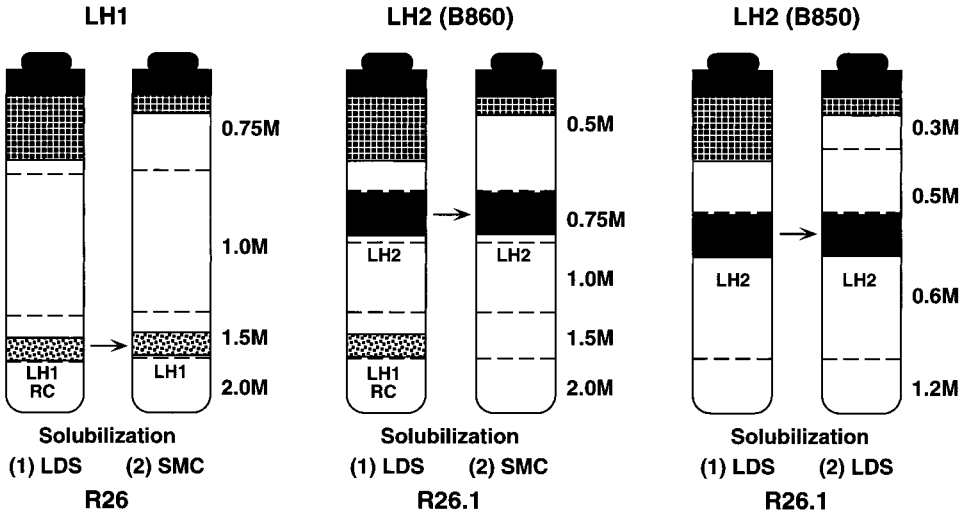

FIGURE 2: The results of sucrose density-gradient centrifugation after (1) the first and (2) the second solubilizations of the LH1, B860 LH2, and B850 LH2 complexes. The sucrose density of each layer and the component of each band are indicated; shadowed top bands are due to denatured components.

LDS and SMC for solubilization and SMC (at a lower concentration) for suspending the resultant LHCs.

The preparation of the LH1 and the LH2 complexes was based on a two-step solubilization using (1) LDS and (2) SMC; each solubilization was followed by fractionation by stepwise sucrose gradient centrifugation (see Materials and Methods).

(a) Preparation of the LH1 Complex. Figure 2 (left) shows a schematic presentation of sucrose density gradient centrifugation after the first (LDS) and the second (SMC) solubilizations. After centrifugation of the first solubilization, the LH1 fraction (dirty green) came down just above the layer of 2.0 M sucrose, but its electronic absorption spectrum (vide infra) showed that the RC complex still remained. (This component can be either the LH1−RC complex or a mixture of the LH1 and RC complexes.) At the top of the tube, denatured components (brownish green) appeared. After centrifugation of the second solubilization, the RC component was completely removed, and the pure LH1 complex (ice blue) appeared above 2.0 M sucrose.

(b) Preparation of a New Type of the LH2 Complex whose Q_y Absorption Appears at 863 nm (We Call this B860 LH2 Complex). The purification procedures were exactly the same as in the case of the LH1 complex except for that we used the chromatophores (OD_{861} = 25 cm^{-1}) from the R26.1 mutant instead of the R26 mutant, and that we purified only the LH2 component. Figure 2 (middle) shows the results of centrifugation of the first (LDS) and the second (SMC) solubilizations. After centrifugation of the first solubilization, a new band (dirty blue) appeared within 0.75 M sucrose; its electronic absorption spectrum and SDS−PAGE showed that it was a crude LH2 component. In addition to this, a band (dirty green) consisting of the LH1 and the RC complexes appeared at the 1.5 M sucrose as in the above case of the R26 mutant; the top band is again a contaminated degradation product (dark dirty green). After centrifugation of the second solubilization of the LH2 component, a pure B860 LH2 complex (ice blue) was obtained.

(c) Preparation of the Traditional B850 LH2 Complex. Here, we repeated twice the LDS solubilization followed by sucrose density gradient centrifugation; Figure 2 (right) shows the results. After centrifugation of the first solubilization, a band of a crude complex (blue) appeared at the top of 0.6 M sucrose; after centrifugation of the second solubilization, a pure B850 LH2 complex (ice blue) was obtained.

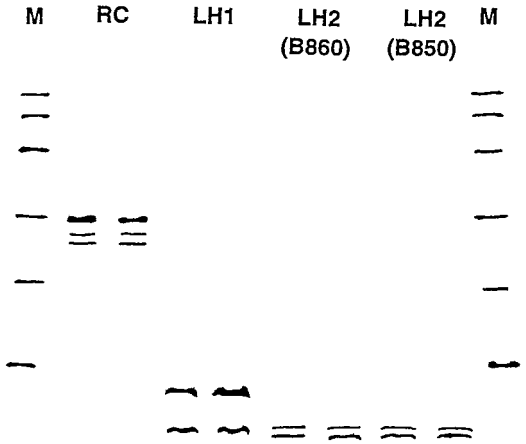

FIGURE 3: The results of SDS−PAGE for the RC, LH1, B860 LH2, and B850 LH2 complexes. The marker proteins (M) include phosphorylase *b* (M_r = 94 000), albumin (67 000), ovalbumin (43 000), carbonic anhydrase (30 000), trypsin inhibitor (20 000), and α-lactalbumin (14 400).

Figure 3 shows the results of SDS−PAGE for the RC, LH1, B860 LH2, and B850 LH2 complexes. On the basis of the molecular weights of the marker proteins (see the caption of Figure 3), the apparent molecular weight on the SDS−PAGE for the α and β subunits could be determined to be 12000 and 8000 for the LH1 complex and 10000 and 8000 for the LH2 complex. The real molecular weights (M_r) for the α and β subunits were determined by amino acid sequencing to be 6809 and 5441 for the LH1 complex and 5647 and 5850 for the LH2 complex (*34*). [The M_r values determined for the H, M, and L subunits of the RC complex were reported to be 28 003 (*35*), 34 265 (*36*), and 31 319 (*37*), respectively.] The electrophoretic patterns prove that we could isolate the LH1 complex and that the peptide subunits of our B860 LH2 complex are the same as those of the traditional B850 LH2 complex. No contaminating peptides are seen for each pigment−protein complex.

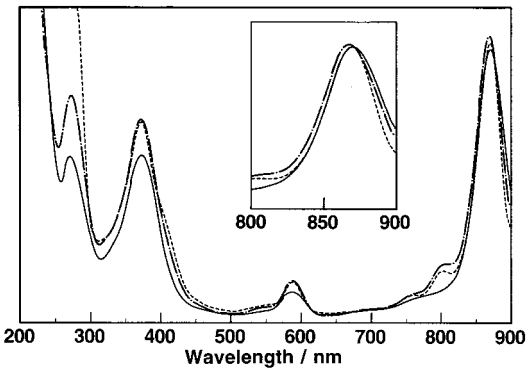

FIGURE 4: The electronic absorption spectra of the LH1 complex (solid line), a crude LH1 + RC component (dotted-broken line), and the chromatophores (broken line) from *R. sphaeroides* R26.

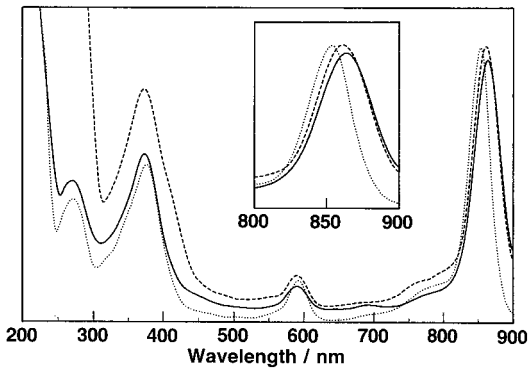

FIGURE 5: The electronic absorption spectra of the B860 LH2 complex (solid line), the B850 LH2 complex (dotted line), and the chromatophores (broken line) from *R. sphaeroides* R26.1.

Table 2: Electronic Absorption Peaks of the Light-Harvesting and the Reaction Center Complexes from *Rhodobacter sphaeroides* R26 and R26.1

		absorption peaks (nm)				intensity ratio
origin	sample	protein	Soret	Q_x	Q_y	protein/Q_y
R26	LH1	271	375	589	873	0.581
	LH1-RC	275	374	589	871 803	0.773
	RC	280	364	597	865 803	1.29
	chromatophores	262	375	590	871	1.380
R26.1	LH2 (B860)	270	375	590	863	0.526
	LH2 (B850)	268	376	593	848	0.419
	RC	279	364	596	864 802	
	chromatophores	258	375	591	861	1.433

Figure 4 compares the electronic absorption spectra of the purified LH1 complex (solid line), a crude "LH1 + RC" component mentioned in the previous section (dotted-broken line), and the chromatophores (broken line), all of which were obtained from the R26 mutant. Table 2 lists the wavelengths of electronic absorption peaks for the above components and the RC; the relative intensity of the protein absorption versus the Q_y absorption is shown in each case. A peak around 800 nm and a weak profile at 760 nm found in the spectra of both the chromatophores and the crude LH1 + RC component indicate that both contain the RC component (vide supra). More importantly, the Q_y absorption of the LH1 complex (873 nm) is very close to that of the chromatophores (871 nm), a fact which shows the integrity of the LH1 complex.

Figure 5 compares the electronic absorption spectra of the B860 LH2 complex (solid line), the B850 LH2 complex (dotted line), and the chromatophores (broken line), all of which originate from the R26.1 mutant. Table 2 lists the wavelengths of electronic absorption peaks for these components and the RC. Although the chromatophores exhibit a pair of peaks around 800 and 760 nm indicating the presence of the RC component, these two peaks are missing in the spectra of both the B860 and the B850 LH2 complexes. Most importantly, the Q_y absorption of the B860 LH2 complex (863 nm) is very close to that of the chromatophores (861 nm). On the other hand, the Q_y absorption of the B850 LH2 complex (848 nm) is shifted to the blue by 13 nm when compared to that of the chromatophores. The Soret and the Q_x absorptions of the B860 LH2 complex are also closer to those of the chromatophores than the B850 LH2 complex. Therefore, the B860 LH2 complex can be regarded as a more native form of the LH2 complex.

Table 3: Classification of the Electronic and the Coordination States of BChl *a* in Terms of the Ring-Breathing Frequency (cm^{-1})[a]

electronic state	penta-coordinated (V)	hexa-coordinated (VI)
ground (S_0)	1611−1605 (12)[b]	1599−1594 (8)
cation radical (D_0)	1599−1595 (7)	1588−1584 (6)
triplet (T_1)	1591−1585 (8)	1581−1578 (5)

[a] From ref *13*. [b] Numer of solvents tested.

Intermolecular Interaction of Ground-State BChl a in the Carotenoidless LHCs As Probed by Ground-State Raman Spectroscopy. The following two different kinds of intermolecular interaction of ground-state BChl *a* can be examined by Raman spectroscopy: (a) The state of coordination of the central Mg atom. The frequency of the 16-membered ring-breathing mode is higher in the pentacoordinated state than in the hexacoordinated state (*38*−*40*). (We define this ring-breathing mode in the ground (S_0) state "ν_r".) Table 3 lists the ν_r frequencies in solutions. The mechanism of the ν_r frequency's reflection of the coordination state can be explained as follows: The Mg atom always has four nitrogen atoms in the macrocycle as ligands, and it can have, in addition, one or two axial ligands (which defines the penta- and hexacoordinated states, respectively). In the pentacoordinated state, the Mg atom sits out of the macrocycle plane; in the hexacoordinated state, it is placed within the macrocycle plane to achieve axial symmetry. In the latter case, the Mg atom expands the conjugated macrocycle and weakens the $C_a'-C_m$ and C_a-C_m bonds (see Figure 1a), and as a result, the ν_r Raman line shifts to the lower frequencies. (b) The state of the keto- and acetyl-carbonyl groups. Hydrogen bonding and ligation of the keto- and acetyl-carbonyl groups can cause polarization of the C═O bond, and as a result, their stretching Raman lines shift to the lower frequencies (hereafter, these modes will be designated "ν_k" and "ν_a", respectively). The ν_k (ν_a) frequency is around 1700−1695 (1660) cm^{-1} when the keto- (acetyl-) carbonyl group is free in a nonpolar environment, while it shifts all the way down to 1648−1640 (1638−1620) cm^{-1} when it is coordinated. Each frequency lies between the above extreme values when it is hydrogen-bonded (*38*, *41*, *42*).

Figure 6 compares the S_0 Raman spectra of the (a) LH1, (b) B860 LH2, (c) B850 LH2 and (d) RC complexes, and (e) BChl *a* in acetone solution (in the pentacoordinated state). This is the first opportunity to examine the Raman spectra

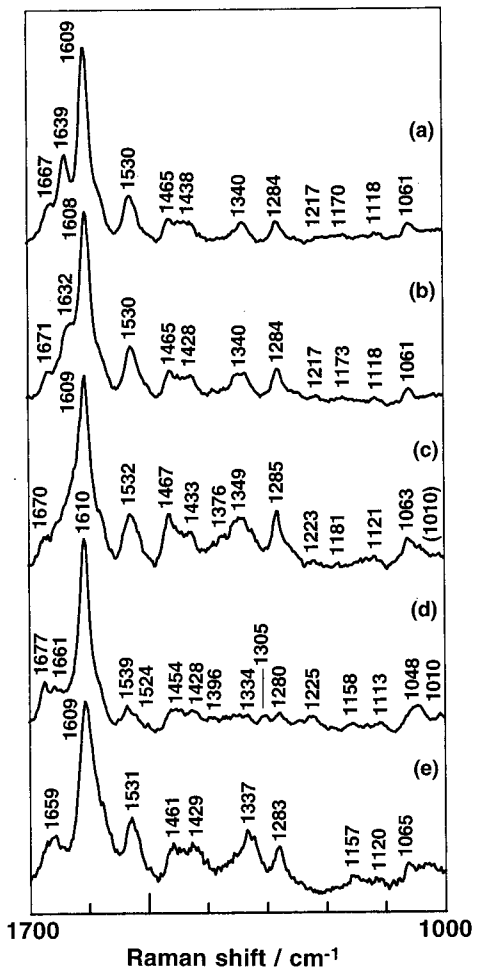

FIGURE 6: The S_0 Raman spectra of the (a) LH1, (b) B860 LH2, (c) B850 LH2, and (d) RC complexes from the carotenoidless mutants of *R. sphaeroides* and (e) BChl *a* in acetone solution. The set of Raman spectra were recorded by using the 355 nm, 12 ns and 10 Hz pulses with low power (2−3 mW, defocused).

of the purified LH1 complex and a native form (B860) of the LH2 complex, both obtained from the carotenoidless mutants of *R. sphaeroides*: (1) The Raman spectral patterns of the LH1 and LH2 complexes are similar to each other. Their ν_r frequencies (1608−1609 cm^{-1}) indicate that the BChl *a* molecules in both LHCs are in the pentacoordinated state. On the basis of the above criteria, the ν_k frequencies (1667 and 1671 cm^{-1} for LH1 and LH2) suggest that the keto-carbonyl groups are hydrogen-bonded. On the other hand, the ν_a frequencies (1639 and 1632 cm^{-1}) suggest that they are hydrogen-bonded, or possibly, coordinated to the Mg atom of the neighboring BChl *a* molecule. (2) Different spectral patterns are found between the LH1 and LH2 complexes in this carbonyl stretching region: The LH1 complex is characterized by a weak ν_k Raman line at 1667 cm^{-1} and a sharp ν_a Raman line at 1639 cm^{-1}, whereas the B860 LH2 complex is characterized by a weak ν_k Raman line at 1671 cm^{-1} and a shoulder ν_a line at 1632 cm^{-1}. (The B850 LH2 complex does not give rise to clear ν_k and ν_a Raman lines, a fact which suggests an inhomogeneous environment of the keto- and the acetyl-carbonyl groups in this particular preparation probably due to its degradation upon laser irradiation.) On the basis of the frequency standards described above, the difference in the ν_k frequency can be ascribed to a difference in hydrogen bonding of the keto-carbonyl group, and the difference in the ν_a frequency can be ascribed to a difference in hydrogen bonding or in the state of ligation of the acetyl-carbonyl group.

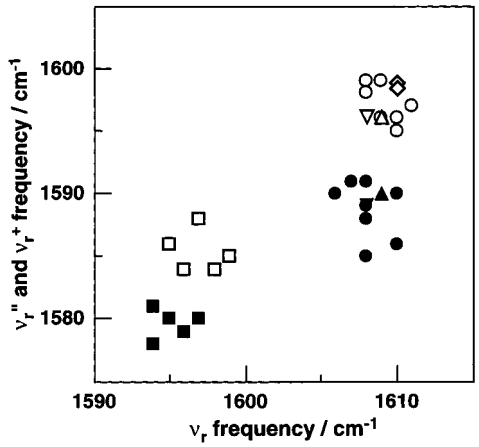

FIGURE 7: Correlation between the ν_r frequency of S_0 BChl *a* and the ν_r'' frequencies of T_1 BChl *a* in the penta- (●) and in the hexa- (■) coordinated states, and correlation between the ν_r frequency and the ν_r^+ frequencies of D_0 BChl *a* cation radical in the penta- (○) and the hexa- (□) coordinated states all in solutions. Correlation between the ν_r and the ν_r'' frequencies for the LH1 (▲) and the LH2 (▼) complexes and correlation between the ν_r and the ν_r^+ frequencies for the LH1 (△), the LH2 (▽), and the RC (◇) complexes are also shown; all of the BChl *a* molecules in the pigment−protein complexes are in the pentacoordinated state. (Modified from Figure 6 of ref *14*.)

Generation of Triplet-State and Cation-Radical BChl a upon Photoexcitation of the Carotenoidless LHCs As Probed by Transient Raman Spectroscopy. The transient species of BChl *a* generated upon photoexcitation of the carotenoidless LHCs can be determined by picosecond and nanosecond transient Raman spectroscopy: As in the S_0 state, the frequency of the ring-breathing Raman line, which appears with the highest intensity when in resonance with the Soret absorption, can be used as a coordination marker in the triplet (T_1) and the cation-radical (D_0) states as well (*13*, *14*, *40*, *43*). (Hereafter, the ring-breathing modes in the S_1, T_1, and D_0 states will be denoted ν_r', ν_r'', and ν_r^+, respectively.) Table 3 lists the ν_r, ν_r^+, and ν_r'' frequencies in different electronic and coordination states. In each electronic state (S_0, D_0, or T_1), the ring-breathing frequencies in the pentacoordinated state (in various solutions) are higher than those in the hexacoordinated state, whereas in each coordination state, the ring-breathing frequencies are in the order $S_0 > D_0 > T_1$. The results support the idea that the same mechanism as in the S_0 state is in operation in the T_1 and D_0 states (the hexacoordinated Mg atom expands the 16-membered ring), and that the size of the 16-membered ring increases in the order $S_0 < D_0 < T_1$. Figure 7 shows the plots of the observed values. The penta- and hexacoordinated states can be clearly distinguished in each of the S_0, D_0, and T_1 states (*13*). [In the S_1 state, the ν_r' frequency was much lower (1575−1567 cm^{-1}), and no difference was seen between the penta- and hexacoordinated states (*14*). The 16-membered ring should be large enough to accommodate the Mg atom in the macrocycle plane even in the pentacoordinated state.]

Figure 8 shows the picosecond transient Raman spectra of (a) the LH1, (b) B860 LH2, and (c) RC complexes: (1) a low-power spectrum, (2) a high-power spectrum, and (3) the difference spectrum of (2) − (1) in a one-color pump-

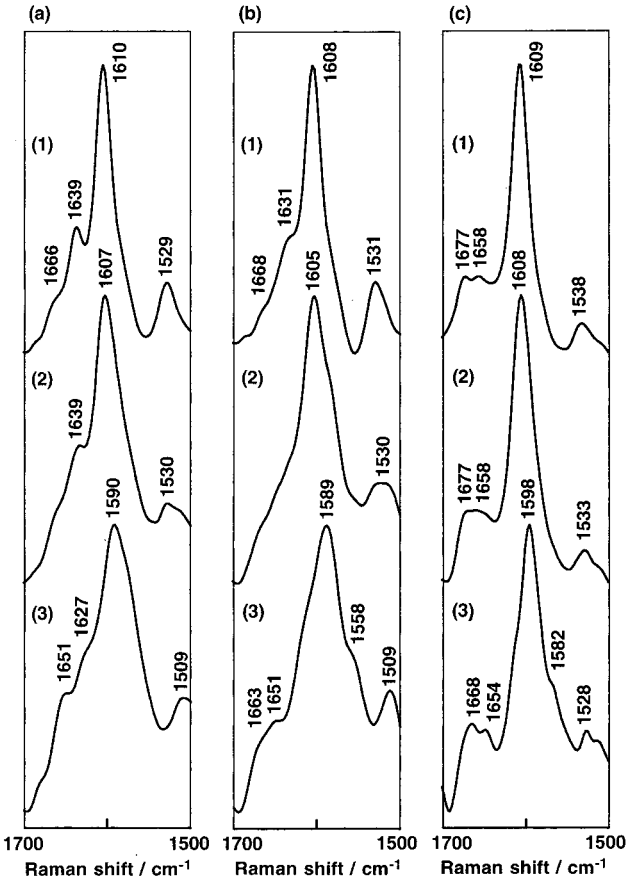

FIGURE 8: The picosecond transient Raman spectra of the (a) LH1, (b) B860 LH2, and (c) RC complexes from the carotenoidless mutants of *R. sphaeroides*: (1) a low-power spectrum (2−3 mW, defocused), (2) a high-power spectrum (25−30 mW, focused), and (3) the difference spectrum of (2) − (1) in a one-color, pump-and-probe experiment using the 351 nm, ∼50 ps, and 1 kHz pulses. The difference spectra are ascribed to the transient species of BChl *a*, that is, the triplet (T_1) state in the LHCs and the cation-radical (D_0) state in the RC.

and-probe experiment using the 351 nm, ∼50 ps pulses. The difference spectra for the LHCs can be ascribed to a transient species of BChl *a*, because it is the only pigment present. In the difference spectra, the LH1 and LH2 complexes exhibit the strongest Raman lines at 1590 and 1589 cm^{-1}, respectively. These frequencies agree with the ring-breathing frequencies of pentacoordinated T_1 BChl *a* in solution (see both Table 3 and the closed triangles in Figure 7). Thus, it is concluded that the T_1 state of BChl *a* is generated in the LHCs upon picosecond pulsed photoexcitation.

In the RC complex, the difference spectrum exhibits a 1598 cm^{-1} Raman line whose frequency agrees with that of a pentacoordinated BChl *a* cation radical (see Table 3 and the open squares in Figure 7). This result indicates that the cation radical of BChl *a* is generated in the RC upon 50 ps pulsed photoexcitation. The possibilities of T_1 and S_1 BPhe are definitely excluded because their ring-breathing frequencies in solutions are 1589−1586 and 1587−1582 cm^{-1}, respectively (*14*). Most probably, the cation radical is generated in the special pair BChls (rather than the accessory BChls) since the charge separation in the special pair is reported to take place within 4 ps and to stay during the pulse duration (*44*−*46*).

Figure 9a−c shows the nanosecond transient Raman spectra of the (a) LH1, (b) B860 LH2, and (c) RC complexes: (1) a low-power spectrum, (2) a high-power spectrum, and (3) the difference spectrum of (2) − (1) in a one-color pump-and-probe experiment using the 355 nm, 12 ns pulses. In both the LH1 and the LH2 complexes, the difference spectra exhibit the strongest Raman lines at 1596 cm^{-1}; the frequency agrees with the ring-breathing frequencies of pentacoordinated BChl *a* cation radicals in solutions (see Table 3 and the open triangles in Figure 7). Therefore, it is concluded that the cation-radical state of BChl *a* is generated in the LHCs upon nanosecond pulsed photoexcitation. In the RC, the pentacoordinated cation-radical state of BChl *a* is generated upon this nanosecond pulsed photoexcitation as in the case of picosecond pulsed photoexcitation (see Table 3 and another open square in Figure 7).

Table 4 summarizes the electronic and the coordination states of BChl *a* bound to the LH1, B860 LH2, and RC complexes: In all of the pigment−protein complexes, the BChl *a* molecules take the pentacoordinated state in the S_0 state. In the LH1 and the LH2 complexes, the T_1 and the D_0 (cation-radical) states of pentacoordinated BChl *a* were generated upon picosecond and nanosecond pulsed photoexcitation, respectively. In the RC, only the D_0 state of pentacoordinated BChl *a* was generated upon either picosecond or nanosecond pulsed photoexcitation.

Figure 9d shows the nanosecond transient Raman spectra of the carotenoid-containing LH2 complex: (1) a low-power spectrum, (2) a high-power spectrum, and (3) the difference spectrum of (2) − (1). The Raman lines at 1589 and 1510 cm^{-1} definitely indicate the generation of the triplet states of BChl *a* and the carotenoid, spheroidene. Most importantly, the cation-radical BChl *a* is not generated when carotenoid is present.

Rapid Generation of Triplet States and Fast Decay of Singlet States upon Photoexcitation of the Carotenoidless and Carotenoid-Containing LHCs As Detected by Subpicosecond to Nanosecond Time-Resolved Absorption Spectroscopy. Identification of the T_1 state of BChl *a* in the carotenoidless LHCs by subpicosecond time-resolved absorption spectroscopy was attempted to confirm the above result of transient Raman spectroscopy; comparison with the case of the carotenoid-containing LH2 complex was also made: Figure 10 shows the subpicosecond to nanosecond time-resolved absorption spectra of (a) the carotenoidless LH1 complex, (b) the carotenoidless B860 LH2 complex, (c) BChl *a* in pyridine solution, and (d) the carotenoid-containing LH2 complex; the 388 nm, 200 fs pulses were used for excitation at the low-energy side of the Soret absorption of BChl *a*. Figure 11 shows the time profiles at different wavelengths for (a) the carotenoidless and (b) the carotenoid-containing LH2 complexes (a logarithmic abscissa scale is used). Since the carotenoidless LH1 and LH2 complexes give rise to similar sets of time-resolved absorption spectra and since the S/N ratio is higher in the latter, we will confine ourselves to describing the results for the LH2 complex; however, the same conclusions can be drawn for the LH1 complex.

The set of time-resolved spectra of the carotenoidless LH2 complex (Figure 10a) shows that most of the transient species decay within the first 10 ps. A broad profile extending over the 400−800 nm region appears at 0.0 ps; dips at 448 and 587 nm can be ascribed to a Raman line of water and the

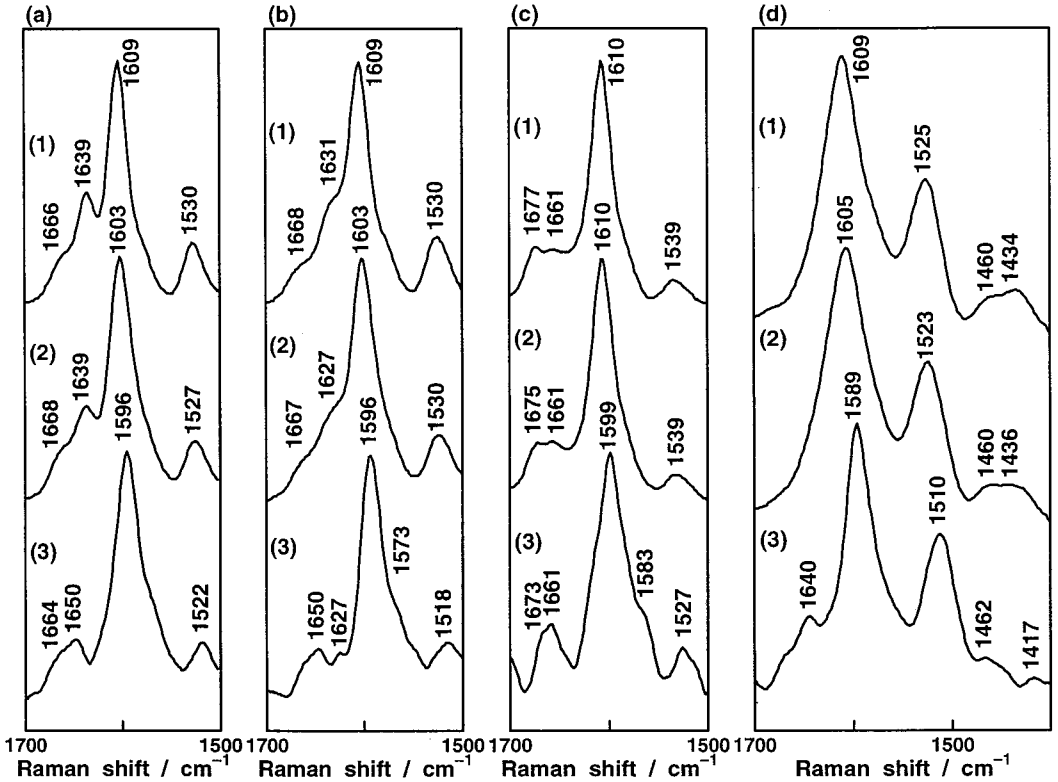

FIGURE 9: The nanosecond transient Raman spectra of the (a) LH1, (b) B860 LH2, and (c) RC complexes from *R. sphaeroides* R 26 and R 26.1 and (d) the LH2 complex from *R. sphaeroides* 2.4.1: (1) a low-power spectrum (2−3 mW, defocused), (2) a high-power spectrum (25−30 mW, focused) and (3) the difference spectrum of (2) − (1) in a one-color experiment using the 355 nm, 12 ns, and 10 Hz pulses. All of the difference spectra (a−c) are ascribed to the cation-radical (D_0) state of BChl *a*, whereas the difference spectrum (d) is ascribed to the triplet states of BChl *a* and the carotenoid (spheroidene).

Table 4: Classification of the Ground (S_0), Triplet (T_1), and Cation-Radical (D_0) States, and of the Penta- (V) and the Hexa-Coordinated (VI) States in Terms of the Ring-Breathing Frequency[a]

sample	S_0 (cm^{-1})	coordination state	T_1 (cm^{-1})	coordination state	D_0 (cm^{-1})	coordination state
LH1	1609	V	1590	V	1596	V
LH2 (B860)	1608	V	1589	V	1596	V
RC (R26)	1610	V			1598, 1599	V

[a] See Table 3 for the notation of the electronic and the coordination states.

bleaching of the Q_x absorption, respectively. The plateau around 640 nm decays faster than the 410 nm peak, and the spectral profile converges to one such as a blow-up at 50 ps, which is very similar to the absorption spectrum of T_1 BChl *a* reported previously (*15*−*17*); see also Figure 12a (vide infra).

The set of time-resolved spectra of BChl *a* in pyridine solution (Figure 10c) shows that a similar spectral pattern persists from the beginning until 1 ns. This spectral pattern can be ascribed in general to a mixture of the S_1 state and the T_1 state of BChl *a*, the latter of which is supposed to be generated by intersystem crossing. The S_1 (Q_y) lifetime in the range 2.3−3.6 ns and the quantum yield of intersystem crossing in the range 0.7−0.9 (*47*) lead us to the time constant of intersystem crossing in the range 2.6−5.1 ns. On the other hand, the lifetime of the Q_x state is in the range 0.1−0.4 ps (*48*). Therefore, the transient absorption spectra in the 10−100 ps time range can be definitely assigned to the $S_n \leftarrow S_1$ absorption, although no authentic $S_n \leftarrow S_1$ absorption spectrum of BChl *a* has been determined except for the 650−950 nm region (*19*). Further, a comparison of this spectrum with the above $T_n \leftarrow T_1$ absorption spectrum leads us to a conclusion that the plateau around 640 nm, the intensity of which is comparable to that of the 420 nm peak, can be regarded as a key absorption in identifying the S_1 state of BChl *a*.

In comparison with the time-resolved spectra of the pyridine solution described above, those of the carotenoidless LH2 (LH1) complex exhibit the following two unique properties (Figures 10a and 11a): (1) most of the transient species decay within a very short period of time after excitation (<10 ps), and (2) the time profile changes depending on the wavelength, suggesting rapid transformation between two different transient species, that is, the S_1 and T_1 states. The time profile of this complex shows clearly that the 640 nm component decays much faster than the 410 nm component as mentioned above. On the basis of the assumptions that the 410 nm peak has contributions from both the S_1 and T_1 states of BChl and that the 640 nm plateau specifically originates from the S_1 state, their time profiles can be explained in terms of rapid generation of the T_1 state which is accompanied by fast decay of the S_1 state.

The spectral changes can be classified as follows (Figure 11a): in the initial 0.3 ps (we call this Phase I), both the 410 and 640 nm components (representing $S_1 + T_1$ and pure S_1 states, respectively) increase; in the next 0.3−0.7 ps (Phase

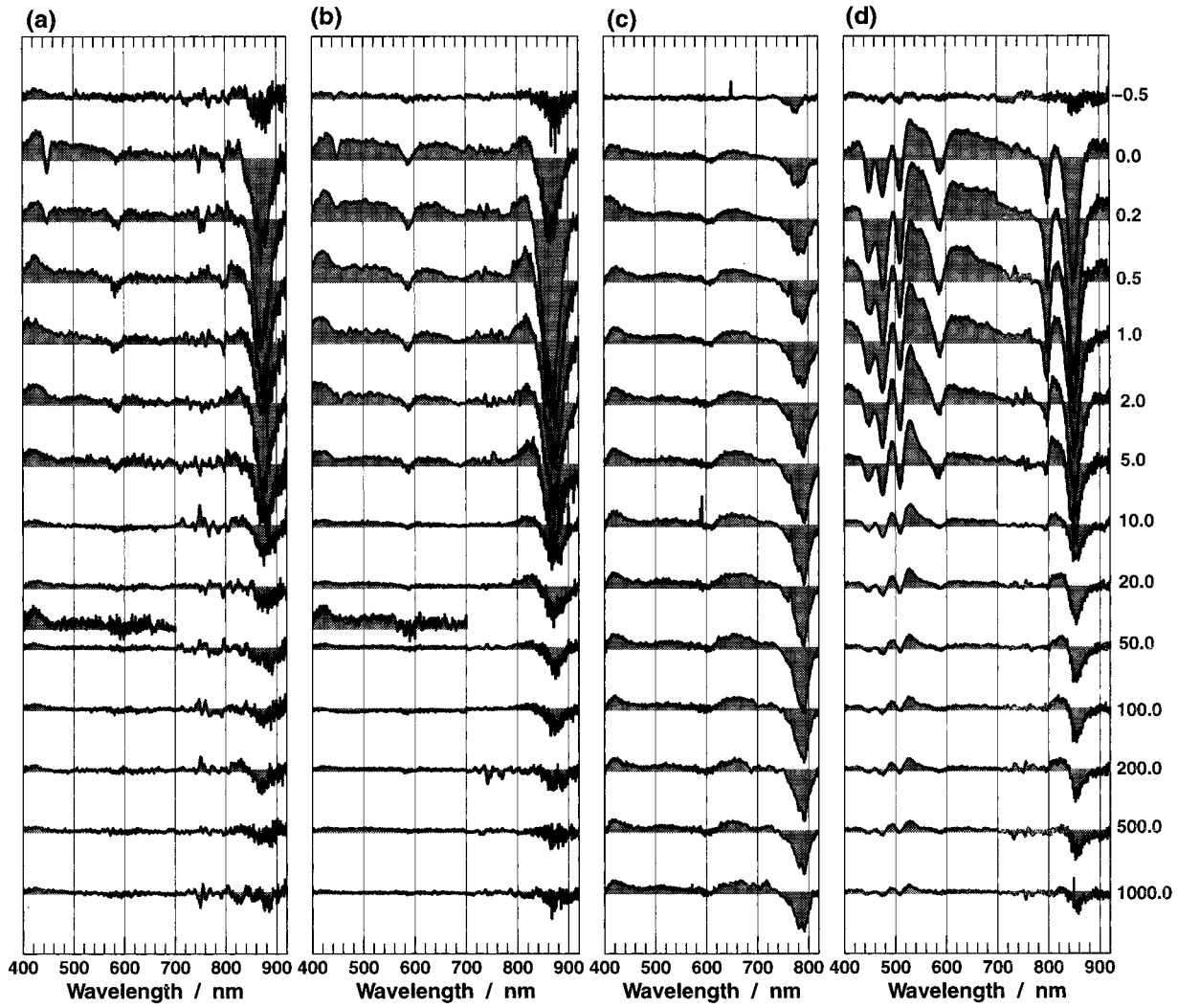

FIGURE 10: Subpicosecond to nanosecond time-resolved absorption spectra of the (a) LH1 and (b) B860 LH2 complexes from *R. sphaeroides* R26 and R26.1, respectively, (c) BChl *a* in pyridine solution, and (d) the LH2 complex from *R. sphaeroides* 2.4.1; 388 nm, 200 fs, and 1 kHz pulses were used for excitation.

F), the 640 nm component (S_1) decreases, whereas the 410 nm component ($T_1 + S_1$) increases further; in the next 0.7−20 ps (Phase A), both the 410 and 640 nm components ($S_1 + T_1$ and S_1) decrease parallel; and after 20 ps (Phase T), the 640 nm component decays to almost 0, whereas the 410 nm component (mainly T_1) remains and then decays much more slowly. In the Discussion, we will correlate Phase F to the generation of the T_1 state through singlet homofission and Phase A to the quenching of the S_1 state through singlet−singlet annihilation. Phase T will be correlated to the long-lived T_1 state which predominates at the later stage.

In the carotenoid-containing LH2 complex also, a majority of the transient species decays within the first 10 ps (Figure 10d); the remaining component in the 500 nm region can be definitely ascribed to the T_1 state of carotenoid (in the subsections of time-resolved absorption spectroscopy, we will denote the relevant carotenoid and BChl *a* as Car and BChl, for simplicity). Surprisingly, the particular 530 nm peak to be assigned to the T_1 state of Car (see also Figure 12e) is clearly seen even at 0.0 ps together with the 410 nm peak due to the $S_1 + T_1$ states of BChl. On the other hand, a shoulder around 560 nm and the 640 profile to be assigned to the S_1 states of Car and BChl, respectively, are also seen. Here again, the wavelength dependence of time profile is clearly observed in both the Car and BChl peaks (Figure 11b): The 560 nm (S_1 Car) and 640 nm (S_1 BChl) components decay faster than the 530 nm (T_1 Car) and 410 nm ($T_1 + S_1$ BChl) components. Thus, the time profiles for the carotenoid-containing LH2 complex can be explained in terms of rapid generation of the T_1 states of both Car and BChl which is accompanied by fast decay of their S_1 states.

The detailed spectral changes can be classified as follows: In the initial 0.4 ps (Phase I), all four components increase together; in the next 0.4−2 ps (Phase F), the 560 nm (S_1 Car) and the 640 nm (S_1 BChl) components start to decrease, whereas the 530 nm component (T_1 Car) and the 410 nm component ($T_1 + S_1$ BChl) continue to increase or stay constant; in the next 2−20 ps (Phase A), all of the components decrease; and in the later period of time (Phase T), all of the 560 nm (S_1 Car), 640 nm (S_1 BChl), and 410 nm ($T_1 + S_1$ BChl) components decay close to 0, whereas the 530 nm component (T_1 Car) stays longer. In the Discussion, we will correlate Phase F to singlet heterofission of S_1 Car and singlet homofission of S_2 BChl, Phase A to singlet−singlet annihilation of S_1 BChl, and Phase T to the quenching of T_1 BChl by Car to generate T_1 Car.

Thus, a major contribution of the T_1 state of BChl *a* in the carotenoidless LH2 complex for the first 50 ps after

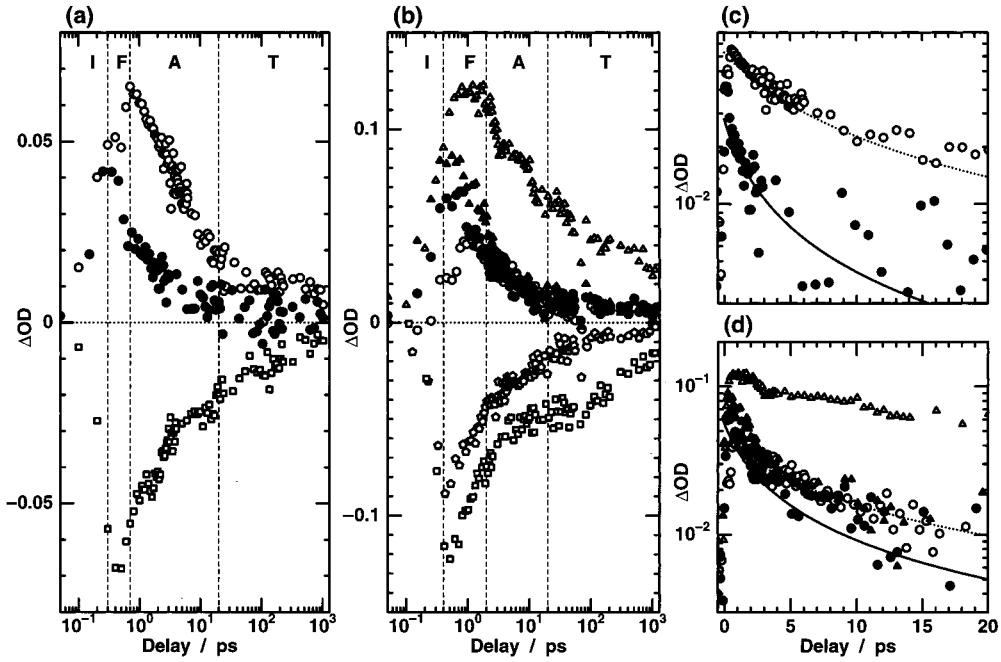

FIGURE 11: (a) Time profiles with a logarithmic abscissa scale for the LH2 complex from *R. sphaeroides* R 26.1 probed at 410 nm (○), 640 nm (●), and 870 nm (□), and (b) those for the LH2 complex from *R. sphaeroides* 2.4.1 probed at 410 nm (○), 640 nm (●), 530 nm (△), 560 nm (▲), 450 nm (⬠), and 850 nm (□). Factors 0.19 and 0.6 were multiplied for the 870 nm (□) and 850 nm (□) bleaching peaks. Different phases, I, F, A, and T are defined (see text). Time profiles with a logarithmic ordinate scale for (c) the LH2 complex from *R. sphaeroides* R 26.1 and (d) the LH2 complex from *R. sphaeroides* 2.4.1 are also shown with fitting curves of the type, $dx/dt = -kx^2$.

photoexcitation has been proved by time-resolved absorption spectroscopy. Rapid generation of the T_1 states of Car and BChl *a* is shown in the carotenoid-containing LH2 complex.

Generation of Triplet-State and Cation-Radical BChl a upon Photoexcitation of the Carotenoidless LHCs As Detected by Microsecond Transient Absorption Spectroscopy. The transformation from the triplet to the cation-radical state of BChl in the LH1 and LH2 complexes was shown by microsecond time-resolved absorption spectroscopy; here again, comparison with the case of the carotenoid-containing LH2 complex was made. Figure 12; parts a and b, show an authentic pair of absorption spectra of T_1 and D_0 (cation-radical) BChl which were generated by photoexcitation of free BChl in pyridine and carbon tetrachloride solutions (*17*) (the bleaching of the S_0-state absorption is compensated to facilitate spectral comparison in the 400 nm region). Figure 12; parts c and d, show the transient absorption spectra of the carotenoidless LH1 and LH2 complexes which were recorded 50 μs after excitation. The strong peaks around 400 and 425 nm can be definitely ascribed to the T_1 and the D_0 states of BChl, respectively. (A pair of dips around 540 nm are ascribable to an artifact which is caused by the fluctuation of the probing Xe flash, the extent of which is comparable to that of the small absorbance changes due to the sample.) Although the origin of the sharp peak around 600 nm is not clear at the present stage, the strong pair of peaks in the 400 nm region definitely indicates that both of the cation-radical and the triplet states of BChl are present. In the carotenoid-containing LH2 complex (Figure 12e), the T_1 state of Car was seen as the major component, and it decayed within 50 μs; the contribution of T_1 BChl is not clear in this spectrum.

Generation of Cation-Radical BChl a upon Photoexcitation of the Carotenoidless LHCs As Proved by EPR Spectroscopy. The EPR signals obtained after photoexcitation of the carotenoidless LHC with a 532 nm, 5 ns pulse provided us with definitive evidence for the generation of the BChl *a* cation radical and information concerning the extent of delocalization of the unpaired electron: Figure 13a compares normalized EPR signals generated photolytically in the LH1 (closed squares), B860 LH2 (closed triangles), and RC (open squares) complexes and BChl *a* in carbon tetrachloride solution (crosses). Table 5 lists their *g* values, peak-to-peak first-derivative line widths (ΔH_{pp}), line shapes, and lifetimes; the measurements were performed at 110 K. All of the *g* values for the pigment−protein complexes and the CCl_4 solution are identical, and they agree with the *g* value of the BChl *a* cation radical obtained by chemical oxidation (vide infra). Further, these *g* values also agree with previously reported values of BChl *a* cation radical (2.0025−2.0026), and all of the *g* values are smaller than those of BChl *a* anion radical (2.0028−2.0035) (*49*). Therefore, the light-induced EPR signals in the pigment−protein complexes can be ascribed to the generation of the BChl *a* cation radical, although the presence of the BChl *a* anion radical cannot be excluded completely because of its similar *g* value. In the case of the RC, the electron ejected from the special-pair BChl *a* is transferred to quinone, and no BChl *a* anion radical is expected to be formed. In the LHCs, the ejected electron is likely to be transferred to the assembly of the BChl *a* molecules and possibly to an amino acid side chain of the apo-peptide.

The line widths of the signals from both LHC complexes are identical (Table 5); they are slightly smaller than that of the RC complex and much smaller than that of the CCl_4 solution. In general, the EPR line width of a radical can be explained in terms of its hyperfine interactions. If the unpaired electron is shared by *N* molecules, the line width can be approximately given as $\Delta H_N = (1/\sqrt{N})\Delta H_M$, where ΔH_M is the line width for a monomer. If one assumes that

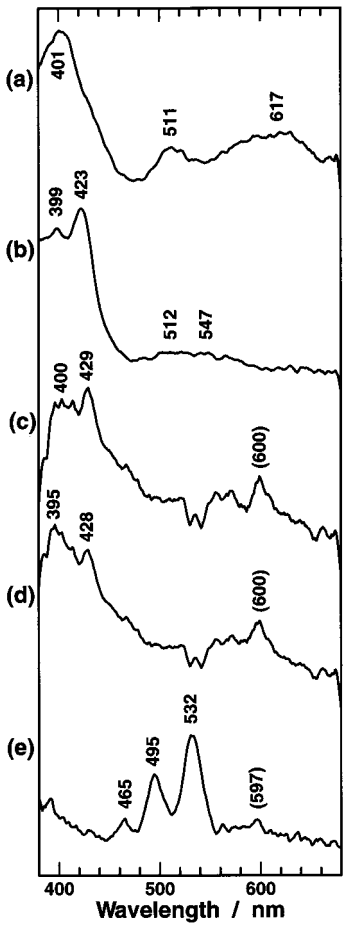

FIGURE 12: Transient absorption spectra of (a) the triplet-state and (b) the cation-radical BChl *a* generated by photoexcitation using the 355 nm, 12 ns, 1 Hz pulses of monomeric BChl *a* in pyridine solution and of BChl *a* aggregates in carbon tetrachloride solution, respectively (both 3×10^{-4} M); 200 ns after excitation. Transient absorption spectra of the carotenoidless (c) LH1 and (d) LH2 complexes from *R. sphaeroides* R 26 and R 26.1 (50 μs after excitation) as well as that of (e) the carotenoid-containing LH2 complex from *R. sphaeroides* 2.4.1 (5 μs after excitation) are also shown.

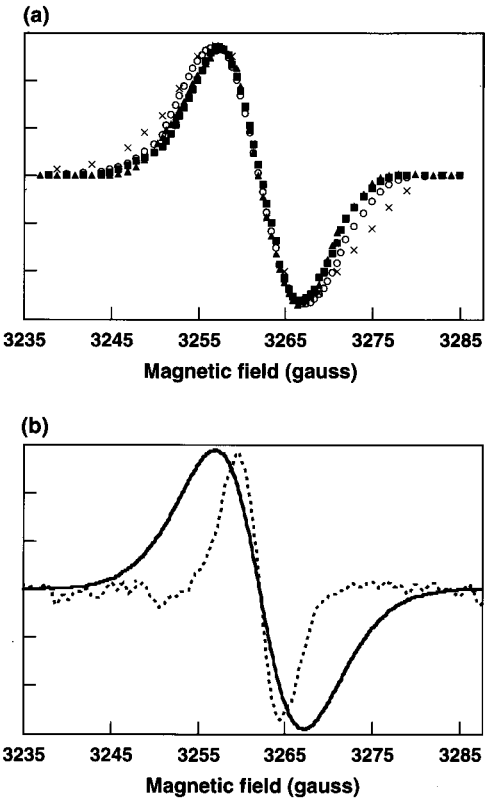

FIGURE 13: (a) Normalized EPR signals from the BChl *a* cation radical generated by photoexcitation using the 532 nm, 5 ns, and 1 Hz pulses of the LH1 complex (■), the B860 LH2 complex (▲), the RC complex (○), and BChl *a* in carbon tetrachloride solution (×). Each point indicates an averaged value (at a given magnetic field) of the peak intensity of a transient signal which was induced by pulsed laser photolysis. (b) EPR signals from the BChl *a* cation radical generated by chemical oxidation of the LH1 complex recorded at 110 K (solid line) and at 296 K (broken line).

Table 5: The *g* Value, the Linewidth, and the Lifetime of the EPR Signals from BChl Cation Radical in the LH1, the B860 LH2, and the RC Complexes and in Carbon Tetrachloride Solution

samples	*g* value	ΔH_{pp}[a] (gauss)	line shape	lifetime (ms)	temperature (K)
LH1	2.0026 ± 0.0002	9.3 ± 0.2	G[b]	27 ± 3	110
LH2 (B860)	2.0026 ± 0.0002	9.3 ± 0.2	G	27 ± 3	110
RC (R26)	2.0026 ± 0.0002	10.3 ± 0.2	G	25 ± 3	110
BChl *a* in CCl_4	2.0026 ± 0.0002	12.3 ± 0.5	G	5 ± 1	110

[a] ΔH_{pp} indicates peak-to-peak first-derivative linewidth. [b] G indicates the Gaussian line shape.

the line width of the CCl_4 solution originates from a monomeric BChl *a* cation radical, then the apparent number of molecules sharing the unpaired electron turns out to be $(12.3/9.3)^2 = 1.75$ in the LHCs and $(12.3/10.3)^2 = 1.42$ in the RC. This assumption is obviously not correct, because BChl *a* is known to form an aggregate in CCl_4; however, the BChl *a* cation radical can never be formed in solvents forming a monomer (*17*). Actually, the EPR signal for the RC has been assigned to the special pair BChl *a*, and the line width of 10.3 G was explained in terms of asymmetric distribution of spin density over the L and M subunits (*50, 51*). On the basis of these results, it can be concluded that the unpaired electrons in the LH1 and LH2 complexes are also shared by at least two nearby BChl *a* molecules probably belonging to the neighboring repeating subunits. This number depends also on the model used in the calculation, that is, either the continuum model or the discrete hopping model (*52*), and therefore, a more detailed analysis is necessary to determine precisely the extent of delocalization of the unpaired electron.

The transient BChl *a* cation radical which is generated by pulsed laser excitation of BChl *a* in the pigment−protein complexes and in the CCl_4 solution must be quenched through charge recombination. The lifetime of the cation radical (Table 5) is in the following order: in CCl_4 solution $\ll$ in the RC $\leq$ in the LHCs. The longer lifetime in the LHCs may reflect larger separation of the pair of cation and anion radicals.

To evaluate the amount of BChl *a* cation radical generated in the LHCs upon pulsed laser photoexcitation at 532 nm, we have determined the intensity of the EPR signal in each of the LHCs relative to that in the RC (we did not try to determine the absolute amounts of the cation radical because the 532 nm excitation may not be so efficient): For the normalized value of 1.0 for the RC at 110 K, the intensities for the LH1 and the LH2 complexes were determined to be 0.1 and 0.08, respectively. If one assumes that the numbers

of BChl *a* molecules in the RC, LH1, and LH2 complexes of the present bacterium are 4, 32, and 18, respectively (see the Introduction), then the ratio of BChl *a* contents in the pigment−protein complexes turns out to be RC/LH1/LH2 = 1:8:4.5. In the EPR measurement, the OD_{max} value of each suspension was equally adjusted to be 100 cm^{-1}. If one takes into account the molar extinction coefficient for the RC, LH1, and LH2, that is, 128 (*53*), 127, and 95 mM^{-1} cm^{-1} (*32*), then the ratio of the BChl *a* concentrations turns out to be RC/LH1/LH2 = 1:1:1.35. Then, the numbers of BChl *a* molecules subjected to the photoexcitation become RC/LH1/LH2 = 1:8:6.1. Thus, the amounts of cation radical generated *per pigment−protein complex* can be determined to be RC/LH1/LH2 = 1:(0.1)(8):(0.08)(6.1). In other words, the generation of the BChl *a* cation radical in the LH1 and LH2 complexes can be estimated to be approximately 80% and 50% of that in the RC. The EPR results indicate that the BChl *a* cation radical can be formed fairly efficiently in the carotenoidless LHCs.

DISCUSSION

Different BChl a−Peptide Intermolecular Interaction in the LH1 and LH2 Complexes. An attempt was made to classify the LH1 and LH2 complexes of various purple photosynthetic bacteria in terms of the frequencies of the keto- and the acetyl-carbonyl stretching Raman lines (*54*). In this study, the authors used the chromatophores from the wild type and the R26 mutant of *R. sphaeroides* for comparison; in the present investigation, their characterization of the Raman spectral patterns is confirmed by the use of the isolated LH1 and LH2 complexes from both of the carotenoidless mutants. In a comparative characterization of the R26 and R26.1 mutants (*12*), the chromatophores of the R26 and R26.1 mutants were used together with the isolated B880 LH1 and B850 and B800−850 LH2 complexes of the wild type then available. The B870 LH1 and the B860 LH2 complexes isolated in the present investigation from the R26 and R26.1 mutants exhibited two clearly distinguishable Raman spectral patterns (Figure 6a,b) which parallel those of the B880 LH1 and the B850 LH2 complexes of the wild type (Figures 2-1 and 2-3 of ref *12*). Thus, the classification of the LH1 and LH2 complexes in terms of the keto- and acetyl-carbonyl stretching (ν_k and ν_a) Raman lines is now established for both the wild type and the carotenoidless mutants. The result strongly supports the idea that the assembly of the B850 BChl molecules is basically the same in each LHC irrespective of the presence or absence of the carotenoid.

Recently, the environment of the keto- and the acetyl-carbonyl groups of BChl *a* in the LHCs was examined in more detail by means of amino acid replacement: In the case of wild-type *R. sphaeroides*, the keto-carbonyl group of B850 BChl *a* was shown to be strongly hydrogen-bonded and the acetyl group is also hydrogen-bonded in the LH2 complex (*55*), whereas both the keto- and the acetyl-carbonyl groups of B880 BChl were shown to be hydrogen-bonded in the LH1 complex (*56*). The X-ray structures of the LH2 complexes from *Rps. acidophila* (PDB 1KZU) and *Rs. molischianum* (PDB 1LGH) provide valuable pieces of information concerning hydrogen bondings: In *Rps. acidophila*, the distance between the keto-carbonyl oxygen of one (the other) B850 BChl *a* and the imidazole nitrogen of the β-30 (α-31 histidine) is 3.50 (3.82) Å, whereas the distance between the acetyl-carbonyl oxygen of one (the other) B850 BChl *a* and the indole nitrogen of the α-45 tryptophan (the phenol oxygen of the α-44 tyrosine) is 2.95 (2.61) Å. In *Rs. molischianum*, the distance between the keto-carbonyl oxygen of one (the other) B850 BChl *a* and the β-35 (α-34) histidine is 3.65 (3.58) Å, whereas the distance between the acetyl-carbonyl oxygen of one (the other) B850 BChl *a* and the indole nitrogen of the α-45 (β-44) tryptophane is 2.73 (2.64) Å. These distances suggest very strong hydrogen bonding of the acetyl-carbonyl group and weaker hydrogen bonding of the keto-carbonyl group, instead. (The possibility of direct ligation of the keto- or the acetyl-carbonyl to the magnesium atom of BChl is excluded on the basis of the X-ray structures.) The above considerations lead us to the conclusion that the difference in the spectral pattern in the C═O stretching region between the LH1 and LH2 complexes (both for the carotenoidless and carotenoid-containing complexes) reflects difference in the strength of hydrogen bondings of the keto- and acetyl-carbonyl groups probably due to the difference in the assembly of the B870 and B850 BChl *a* molecules.

Possible Mechanisms for the Rapid Generation of the Triplet State and the Fast Decay of the Singlet State of BChl a upon Photoexcitation of the Carotenoidless LH2 Complex. X-ray crystallography of the carotenoid-containing LH2 complexes from *Rps. acidophila* and *Rs. molischianum* has provided the following information concerning close contacts among the B850 BChl and Car molecules. (1) Carbon−carbon contacts between the neighboring B850 BChl molecules: concerning the contact within the repeating subunits, the distance between $C13^1$ and $C13^2$ is 3.47 Å in *Rps. acidophila* (PDB 1KZU) and 3.43 Å in *Rs. molischianum* (PDB 1LGH); and concerning contact between the neighboring repeating subunit, the distance between C1 and C2 is 3.84 Å in *Rps. acidophila* (PDB 1KZU) and 3.54 Å in *Rs. molischianum* (PDB 1LGH). (2) Carbon−carbon contacts between the Car and B850 BChl molecules: the distance between C-4 of Car (rhodopin glucoside) and C-20 of B850 BChl is 3.64 Å in *Rps. acidophila* 10050 (PDB 1KZU); and the distance between C-4 of Car (lycopene) and C-20 of B850 BChl is 3.60 Å in *Rs. molischianum* (PDB 1LGH).

To interpret various phases of spectral changes observed in the subpicosecond to nanosecond time-resolved absorption spectroscopy of the carotenoidless LH2 complexes (see the Results), we will tentatively propose possible mechanisms on the basis of the assumption that the assembly of the BChl molecules in the carotenoidless LH2 complex of *R. sphaeroides* should be basically the same as that in the carotenoid-containing LH2 complexes: When the BChl molecule was excited at the low-energy side of the Soret absorption, Phase F where the 640 nm component of S_1 BChl decreases and the 410 nm component representing T_1 (+ S_1) BChl increases was observed (Figure 11a). This phase can be explained in terms of internal conversion to the Q_x state, which is followed by singlet homofission with ground-state (S_0) BChl

$$^1\text{BChl}^*(\text{Soret}) \rightarrow {}^1\text{BChl}^*(Q_x) \quad (1)$$

$$^1\text{BChl}^*(Q_x) + {}^1\text{BChl}(S_0) \rightarrow 2 \times {}^3\text{BChl}^*(T_1) \quad (2)$$

Here, the T_1 state can be generated at the expense of the S_1

state (note that the total number of excited-state BChl is doubled) in this fission reaction, which is based on electron exchange between a pair of BChl molecules. The following conditions are the bases for the proposition of this mechanism: (a) Since the Q_y absorption and the Raman spectral pattern of this complex suggest that the macrocycles of the B850 BChl molecules are stacked together to form a circular aggregate to facilitate close contacts among them, just as in the case of the carotenoid-containing LH2 complexes (see above for those close contacts between a pair of B850 BChl molecules in the carotenoid-containing LH2 complexes of *Rps. acidophila* and *Rs. molischianum*), the spatial condition for this reaction must be satisfied. (b) The Q_x energy of 16900 cm^{-1} is slightly higher than twice the T_1 energy, that is, $8200 \times 2 = 16\,400$ cm^{-1} (*57*), a fact which satisfies the energetic condition of the reaction. (c) A large excess energy which was deposited on the low-energy side of the Soret absorption (25 800 cm^{-1}) with the time duration of 0.2 ps may provide enough time for this reaction to take place in the time range of this phase F, 0.3−0.7 ps. Even when the Q_x absorption was excited directly, its lifetime for the internal conversion to the Q_y state was reported to be 0.1−0.4 ps (*48*). (One of the reviewers questioned this singlet homofission mechanism, because the transient absorption spectrum at −0.5 ps in Figure 10a shows an indication of T_1 BChl *a* just like the spectrum at 20 ps, for example. We tried to reduce the repetition rate from 1 kHz to 100 Hz, but the S/N ratio of the resultant time-resolved spectra was too low to evaluate the accumulated triplet species. The final conclusion should wait for further investigation.)

Phase A where both the 640 nm component of S_1 BChl and the 410 nm component of S_1 (+ T_1) BChl decay parallel to each other can be explained in terms of singlet−singlet annihilation

$$^1\text{BChl}^*(Q_y) + {}^1\text{BChl}^*(Q_y) \rightarrow {}^1\text{BChl}(S_0) + {}^1\text{BChl}^*(2Q_y) \rightarrow {}^1\text{BChl}(S_0) + {}^1\text{BChl}^*(Q_y) \quad (3)$$

The S_1 state of BChl can be quenched very efficiently in this annihilation reaction, which is based on interaction between the transition dipoles of the neighboring B850 BChl molecules. The following conditions are expected to facilitate this annihilation reaction: (a) The Q_y transition dipoles of the B850 BChl molecules must be parallel to each other as in the case of the carotenoid-containing LH2 complexes of *Rps. acidophila* and *Rs. molischianum* (*1*−*5*). (b) The strong negative peak around 870 nm which is ascribable to the $S_1 \leftarrow S_0$ ($Q_y \leftarrow S_0$) absorption (and possibly to the $S_1 \rightarrow S_0$ stimulated emission) as well as the weak positive peak around 820 nm which has been assigned to the $2Q_y \leftarrow Q_y$ absorption (*58*) indicate highly populated S_1 BChl at an initial stage. (c) The latter optically active $S_2 \leftarrow S_1$ transition must facilitate the first reaction in eq 3.

Equation 3 shows that the singlet−singlet annihilation reaction must exhibit a unique property of a bimolecular, second-order reaction. On the other hand, the singlet−triplet annihilation reaction

$$^1\text{BChl}^*(Q_y) + {}^3\text{BChl}^*(T_1) \rightarrow {}^1\text{BChl}(S_0) + {}^3\text{BChl}^*(T_n) \rightarrow {}^1\text{BChl}(S_0) + {}^3\text{BChl}^*(T_1) \quad (4)$$

and all of the other reactions listed in this section are first-order reactions for each component. When a logarithmic ordinate scale is taken in the time profile, the first-order reaction should give rise to a straight line, whereas the second-order reaction should exhibit a concave curve. Therefore, the singlet−singlet annihilation reaction can be identified by the analysis of such a time profile. Figure 11c shows that the time profile of the 640 nm component representing S_1 BChl as well as that of the 410 nm component representing S_1 (+ T_1) BChl (note that the amount of T_1 BChl changes little in this picosecond time scale) can be fit not by a straight line but by a curve expressing the relation, $dx/dt = -kx^2$, where x is the amount of S_1 BChl. This fact provides a strong support that the singlet−singlet annihilation reaction predominates in this time scale.

In Phase T, the 640 nm component of S_1 BChl decays to practically 0, and the 410 nm component of T_1 BChl alone decays slowly.

Possible Mechanisms for the Rapid Generation of the Triplet States and the Fast Decay of the Singlet States of BChl a and Spheroidene upon Photoexcitation of the Carotenoid-Containing LH2 Complex. When BChl was excited at the low-energy side of the Soret absorption, Phase I where the 410 nm component of S_1 BChl and the 560 nm component of S_1 Car increase in parallel was observed (Figure 11b). This phase can be explained in terms of BChl-to-Car singlet-energy transfer,

$$^1\text{BChl}^*(\text{Soret}) + {}^1\text{Car}(S_0) \rightarrow {}^1\text{BChl}(S_0) + {}^1\text{Car}^*(B_u^+) \quad (5)$$

which is based on instantaneous interaction between the transition dipoles of the BChl and Car molecules. The following energetic and spatial conditions should facilitate this efficient singlet-energy transfer: (a) The energy of the emissive Soret $\rightarrow S_0$ transition of BChl (excitation at 25 800 cm^{-1}) and the energy of the absorptive $B_u^+ \leftarrow S_0$ transition of Car (19 600 cm^{-1} for $v = 0$) overlap with each other. (b) The BChl and Car molecules are located side-by-side (see above for the contact between these molecules). (c) The transition moment of the lower component of the Soret transition is along the x axis of the BChl macrocycle (*59*), and the B_u^+ transition moment is along the long axis of the Car conjugated system. Therefore, these transition moments are expected to be parallel in the present carotenoid-containing LH2, just as in the case of those of *Rps. acidophila* and *Rs. molischianum* (*1*−*5*).

Phase F, where the 560 nm component of S_1 Car and the 640 nm component of S_1 BChl decrease, whereas the 530 nm component of T_1 Car and the 410 nm component of T_1 (+ S_1) BChl component increase or stay at a constant level, can be explained in terms of singlet heterofission after the internal conversion of Car to the $2A_g^-$ state

$$^1\text{Car}^*(B_u^+) \rightarrow {}^1\text{Car}^*(2A_g^-) \quad (6)$$

$$^1\text{Car}^*(2A_g^-) + {}^1\text{BChl}(S_0) \rightarrow {}^3\text{Car}^*(T_1) + {}^3\text{BChl}^*(T_1) \quad (7)$$

(A singlet homofission reaction through the $2A_g^-$ state of Car, to generate two T_1 Car, can be proposed if the two Car

molecules are in contact in the LH2 complex, because the $2A_g^-$ electronic structure has a nature of double $^3B_u^+$ electronic excitation (*60*). However, the present X-ray results completely exclude the possibility of close contact between a pair of carotenoid molecules.) The T_1 states of both Car and BChl can be generated at the expense of S_1 Car in this heterofission reaction, which is based on electron exchange between the Car and BChl molecules. The conditions for this heterofission reaction are considered to be satisfied as follows: (a) Spatially, the Car and BChl molecules are in contact with each other in the carotenoid-containing LH2 complexes of *Rps. acidophila* and *Rs. molischianum* (vide supra). (b) Energetically, the $v = 1$ level of the $2A_g^-$ state of Car ($14\,200 + 1500 = 15\,700$ cm^{-1}) is slightly higher than a sum of the T_1 energies of Car and BChl ($7100 + 8200 = 15\,300$ cm^{-1}). (c) Temporally, the $2A_g^-$ lifetime of 2.0 ps (our observation) and time for vibrational relaxation in the $2A_g^-$ state of lycopene, 10^1 ps (*61*), seem to provide more than enough time for this fission reaction to take place (time range of Phase F, 0.4−2 ps). When the B_u^+ state of Car was excited in another experiment, the $S_n \leftarrow S_1$ ($2B_u^+ \leftarrow 2A_g^-$) absorption was observed at 0.0 ps, and then, the $T_n \leftarrow T_1$ absorption appeared at 0.2 ps after excitation. This set of observations seems to support the above singlet heterofission reaction through the $2A_g^-$ (S_1) state of Car. When the Q_x or Q_y state of BChl was excited, no generation of T_1 Car was observed.

Generation of T_1 BChl in Phase F can also be explained by singlet homofission between the neighboring B850 BChl molecules as in the case of the carotenoidless antenna complex (eq 2).

Phase A where the 410 component of S_1 (+ T_1) BChl and the 640 nm component of S_1 BChl decrease in parallel can be explained, again, in terms of the singlet−singlet annihilation reaction between the B850 BChl molecules (eq 3). The time profiles with a logarithmic ordinate scale for this LH2 complex (Figure 11d) show that the decay of both the 640 nm and the 410 nm components can be fit as a second-order reaction, a fact which indicates that this phase represents the singlet−singlet annihilation reaction between the two S_1 BChl molecules.

Phase T, where the 410 nm component of T_1 BChl disappears, whereas the 530 nm component of T_1 Car stays longer, can be explained in terms of BChl-to-Car triplet-energy transfer,

$$^3\text{BChl}^*(T_1) + {}^1\text{Car}(S_0) \rightarrow {}^1\text{BChl}(S_0) + {}^3\text{Car}^*(T_1) \quad (8)$$

in which T_1 BChl is replaced by T_1 Car. Here again, the close contact between the Car and BChl molecules mentioned above must facilitate this efficient triplet-energy transfer reaction through electron exchange.

Thus, the wavelength-dependent time profiles have been explained in terms of transitions among the S_0, S_1, and T_1 states of BChl and Car through the (1) singlet homo- and hetero-fission, (2) singlet−singlet annihilation, and (3) singlet and triplet energy-transfer reactions based on the unique assembly of the pigment molecules in the LHCs.

The present observation of the singlet homo- and hetero-fission as well as of the singlet−singlet annihilation reactions can be compared (contrasted) to the results of previous investigations as follows: (1) Generation of T_1 BChl through intersystem crossing from S_1 BChl and subsequent generation of T_1 Car through BChl-to-Car triplet-energy transfer were first detected by transient absorption spectroscopy of the carotenoidless and the carotenoid-containing chromatophore membranes of the present organism (*62*, *63*). Both T_1 BChl and T_1 Car were detected after excitation with 694 nm, 15−20 ns pulses, and the time for the triplet-energy transfer was determined to be ∼20 ns. The quenching of S_1 BChl by these triplet species through singlet−triplet annihilation was also identified in the microsecond time scale. (2) Then, a completely different type of triplet generation which is relevant to the present observation was found: When the B_u^+ state of Car (spirilloxanthin) in the chromatophores of *Rs. rubrum* was excited with 532 nm, 35 ps pulses, the generation of T_1 Car was observed within 100 ps (*64*). This fast generation of T_1 Car was ascribed to singlet homo- or hetero-fission of S_1 Car. The magnetic field dependence in fluorescence (*65*) and transient absorption (*66*) for the carotenoidless and carotenoid-containing chromatophores and cells provided a strong support for this fission mechanism; the homofission mechanism was proposed for *R. sphaeroides*, whereas the hetero-fission mechanism was proposed for *Rs. rubrum*. (3) Photon-density-dependent decrease in fluorescence lifetime and in fluorescence quantum yield was observed when the carotenoidless and the carotenoid-containing chromatophore membranes of the present organism were excited with 530 nm, 20 ps pulses (*67*). This observation was ascribed to singlet−singlet annihilation (see also a review by van Grondelle, ref *68*). Later, the decrease in fluorescence quantum yield as a function of the photon density was used to estimate the number of interacting BChl molecules in the LH2 complexes of *Rs. rubrum* and *Rhodobacter capsulatus* (*69*). The above picosecond absorption spectroscopy of the *Rs. rubrum* chromatophores (*64*) also detected the shortening of the lifetime of S_1 BChl from ∼350 ps to less than 10 ps when the photon density was increased. Most recently, this singlet−singlet annihilation process was used, together with time-resolved fluorescence anisotropy measurement, in modeling the interactions of the BChl molecules in the LH1 complex of the present organism (*70*).

The present results and interpretation are consistent with those of the previous investigations. The uniqueness of the present investigation is the usage of the wavelength-dependent time profiles in the identification of those fission and annihilation reactions in the carotenoidless and carotenoid-containing LHCs of *R. sphaeroides*.

Detection of T_1 BChl as the major component in the carotenoidless LHCs by transient Raman spectroscopy using 50 ps pulses is consistent with the results of subpicosecond to picosecond time-resolved absorption spectroscopy using 0.2 ps pulses. The time-resolved absorption spectroscopy showed that S_1 BChl decays almost completely within the first 10 ps, and that T_1 BChl becomes the major component in the rest of the 40 ps when excited with a 0.2 ps pulse. However, quantitative comparison of the results obtained by the two spectroscopic methods is extremely difficult, even though the applied photon densities (10^{15} photon·pulse^{-1}·cm^{-2}) and the ratios of the number of photons versus the number of molecules irradiated (∼1) are approximately the same. In particular, the relative Raman intensity of the S_1 and T_1 states strongly depends on the resonance conditions, a

comparison of which is now impossible because the molecular extinction coefficient of the $S_n \leftarrow S_1$ absorption in the Soret region has not been determined.

Generation of BChl a Cation Radical by Photoexcitation of BChl a Aggregates in Solution: Comparison with Photoexcitation of the Carotenoidless LHCs. When BChl *a* in THF solution was excited and probed by the 355 nm, 12 ns pulses, the T_1 state was generated (*30*). The T_1 state was always detected for monomeric BChl *a* in solution by both transient Raman (*40*) and transient absorption (*17*) spectroscopies using nanosecond pulses. However, when BChl *a* was dissolved in methylene chloride (forming a pentacoordinated lower aggregate), transformation from the T_1 state into the D_0 (cation-radical) state was detected by time-resolved absorption spectroscopy in the submicrosecond to 100 microsecond time scale. Further, when BChl *a* was dissolved in carbon tetrachloride (forming a pentacoordinated higher aggregate), the cation-radical state was generated within 200 ns (*17*).

It is not surprising that the cation-radical state can be generated in the carotenoidless LHCs, when the B850 BChl molecules which are stacked together to form a circular aggregate are excited to the triplet state, because electron transfer from one BChl molecule to another (most probably between the neighboring repeating subunits) can be naturally expected. Therefore, the light-induced cation-radical formation in the carotenoidless LHCs can be regarded as reflection of the unique assembly of the B850 BChl molecules just as the generation of the triplet state through the singlet-homofission reaction. In the presence of Car, the triplet-state BChl *a* is quenched, and therefore, the light-induced cation-radical formation is prevented.

In the present case of the carotenoidless LHCs, the cation-radical state was detected as the major component by transient Raman spectroscopy using the 355 nm, 10 Hz, 12 ns pulses, whereas both the cation-radical and the triplet states were detected by microsecond time-resolved absorption spectroscopy using the same pulses except for the lower repetition rate (1 Hz). Since the molar extinction coefficients at 355 nm for the triplet state, 1.5×10^4 $M^{-1}cm^{-1}$ (*15*), and the cation-radical state, 2.0×10^5 $M^{-1}cm^{-1}$ (*18*), are on a similar order of magnitude, the selective detection of the cation-radical state by transient Raman spectroscopy may be due to its accumulation of a component living longer than the repetition interval of 100 ms (10 Hz), although time-resolved EPR spectroscopy using 532 nm, 1 Hz, and 5 ns pulses determined its lifetime to be 27 ms.

Generation of BChl a Cation Radical by Chemical Oxidation of the LHCs: Comparison with Photo-oxidation. The generation of BChl *a* cation radical upon chemical oxidation of the LHCs using ferricyanide was first evidenced by EPR and electronic absorption spectroscopies for the chromatophores of the RC-less mutant of *Rs. rubrum* (*71*); a Gaussian signal with a *g* value of 2.0025 and a line width of 3.8 G was detected. Similar observations were made for the purified LH1 complexes of *Rs. rubrum*, *R. sphaeroides*, and *Ectothiorhodospira* sp. (*72*) as well as for the chromatophores of *R. capsulatus* (*73*) and another RC-less mutant of *Rs. rubrum* (*74*). In all of the above cases of chemical oxidation, the line width was in the range 3.6−4.8 G, and the application of the equation, $\Delta H_N = (1/\sqrt{N})\Delta H_M$ (vide supra), leads us to the apparent number of BChl *a* molecules (*N*) sharing the unpaired electron in the range 7−12. Recently, the temperature dependence of the EPR line width was found for the LH1 complex of wild-type *R. sphaeroides*, where the line width was broadened from 4.1 G at room temperature to 10.0 G at 4.0 K (*75*). The results have been explained in terms of the electron hopping mechanism (*52*) instead of the above continuous mechanism.

For comparison, we conducted a similar experiment using the newly prepared LH1 complex from the carotenoidless mutant of *R. sphaeroides* R26: Figure 13b shows the EPR signals obtained by the chemical oxidation of this LH1 complex using potassium cyanide at 110 K (solid line) and 296 K (broken line). The *g* value was 2.0026 ± 0.0002. The line width of 10.4 ± 0.1 G at 110 K decreased down to 4.7 ± 0.3 G at room temperature. The results parallel those of the above wild-type LH1 complex reported previously.

In the present carotenoidless LH1 complex, the temperature dependence of cation-radical formation by photo-oxidation can be contrasted to that by chemical oxidation as follows: In chemical oxidation, the intensity of the signal was reduced into 17% and the line width was decreased from 10.4 to 4.7 G on going from 110 K to room temperature. In photo-oxidation, no EPR signal was detected at room temperature, but it became detectable at 250 K. The signal intensity was reduced into 4% on going from 110 to 250 K, but no changes were observed either in line width or in lifetime.

The above difference can be explained in terms of different mechanisms of BChl *a* cation-radical formation: In chemical oxidation, the cation radical is formed as a *stationary-state* species, because the ejected electron is trapped strongly by the oxidant, ferricyanide. The unpaired electron is shared by a BChl pair at 4 K and by 7−12 BChl molecules at room temperature. Therefore, the temperature dependence is mainly related to the extent of delocalization of the unpaired electron of the stationary-state cation radical. In photo-oxidation, on the other hand, the cation radical is formed as a *transient* species which is destined to disappear in the time scale of 27 ms through charge recombination. Therefore, the temperature dependence is related to the efficiency of charge recombination between the transient cation radical and its counterpart; here, the extent of delocalization of the unpaired electron of the cation radical is always limited within, or slightly over, the BChl *a* pair covering the neighboring repeating subunits.

CONCLUSIONS

The LH1 complex and a native form of the LH2 complex have been isolated from the carotenoidless mutants of *R. sphaeroides* and characterized. Transient Raman spectroscopy of the LHCs detected both the generation of the triplet state upon picosecond pulsed photoexcitation and the generation of the cation-radical state upon nanosecond pulsed photoexcitation. Subpicosecond to picosecond time-resolved absorption spectroscopy revealed rapid generation of the triplet state and fast decay of the singlet state. Submicrosecond to microsecond time-resolved absorption spectroscopy showed transformation of the triplet state into the cation-radical state. EPR spectroscopy confirmed the generation of the cation radical and showed that the unpaired electron is

shared by two BChl *a* molecules. The yields of the BChl *a* cation radical per pigment−protein complex in the LH1 and the LH2 complexes have been estimated to be about 80% and 50% of that in the RC. The generation of the triplet state is ascribed to singlet homofission and the generation of the cation-radical state to charge separation, both between the BChl pair covering the neighboring repeating subunits in the LHCs. Thus, these reactions, when an excess amount of photons is applied, originate from the unique assembly of the B850 BChl *a* molecules.

The generation of the triplet state of BChl *a* and the subsequent transformation into the cation-radical state have been shown as intrinsic properties of the isolated, carotenoidless antenna complexes. In the carotenoid-containing LH2 complex, the cation-radical state of BChl *a* cannot be generated because the triplet state of BChl *a* is quenched by carotenoid. Thus, the photoprotective function of carotenoid against the photo-oxidation of BChl *a* is evidenced.

ACKNOWLEDGMENT

The authors thank Mr. Hideo Ishiwatari for synthesizing sucrose monocholate. The authors are indebted to Prof. Hiroyoshi Nagae for stimulating discussion and for reading the manuscript.

REFERENCES

1. McDermott, G., Prince, S. M., Freer, A. A., Hawthornthwaite-Lawless, A. M., Papiz, M. Z., Cogdell, R. J., and Isaacs, N. W. (1995) *Nature 374*, 517−521.
2. Papiz, M. Z., Prince, S. M., Hawthornthwaite-Lawless, A. M., McDermott, G., Freer, A. A., Isaacs, N. W., and Cogdell, R. J. (1996) *Trends Plant Sci. 1*, 198−206.
3. Freer, A., Prince, S., Sauer, K., Papiz, M., Hawthornthwaite-Lawless, A., McDermott, G., Cogdell, R., and Isaacs, N. W. (1996) *Structure 4*, 449−462.
4. Prince, S. M., Papiz, M. Z., Freer, A. A., McDermott, G., Hawthornthwaite-Lawless, A. M., Cogdell, R. J., and Isaacs, N. W. (1997) *J. Mol. Biol. 268*, 412−423.
5. Koepke, J., Hu, X., Muenke, C., Schulten, K., and Michel, H. (1996) *Structure 4*, 581−597.
6. Karrasch, S., Bullough, P. A., and Ghosh, R. (1995) *EMBO J. 14*, 631−638.
7. Sauer, K., Cogdell, R. J., Prince, S. M., Freer, A., Isaacs, N. W., and Scheer, H. (1996) *Photochem. Photobiol. 64*, 564−576.
8. Kühn, O., Chernyak, V., and Mukamel, S. (1996) *J. Chem. Phys. 105*, 8586−8601.
9. Kühn, O., and Mukamel, S. (1997) *J. Phys. Chem. B 101*, 809−816.
10. Alden, R. G., Johnson, E., Nagarajan, V., Parson, W. W., Law, C. J., and Cogdell, R. J. (1997) *J. Phys. Chem. B 101*, 4667−4680.
11. Hu, X., Damjanovic, A., Ritz, T., and Schulten, K. (1998) *Proc. Natl. Acad. Sci. U.S.A. 95*, 5935−5941.
12. Robert, B., Vermeglio, A., and Lutz, M. (1984) *Biochim. Biophys. Acta 766*, 259−262.
13. Koyama, Y., Limantara, L., Nishizawa, E., Misono, Y., and Itoh, K. (1995) Proceedings of the 7th International Conference on Time-Resolved Vibrational Spectroscopy, pp 45−49, Los Alamos National Laboratory, Santa Fe, New Mexico.
14. Koyama, Y., and Limantara, L. (1998) *Spectrochim. Acta, Part A 54*, 1127−1139.
15. Pekkarinen, L., and Linschitz, H. (1960) *J. Am. Chem. Soc. 82*, 2407−2416.
16. Connolly, J. S., Gorman, D. S., and Seely, G. R. (1973) *Ann. N. Y. Acad. Sci. 206*, 649−669.
17. Nishizawa, E., Nagae, H., and Koyama, Y. (1994) *J. Phys. Chem. 98*, 12086−12090.
18. Cotton, T. M., Parks, K. D., and van Duyne, R. P. (1980) *J. Am. Chem. Soc. 102*, 6399−6407.
19. Becker, M., Nagarajan, V., and Parson, W. W. (1991) *J. Am. Chem. Soc. 113*, 6840−6848.
20. Broglie, R. M., Hunter, C. N., Delepelaire, P., Niederman, R. A., Chua, N.-H., and Clayton, R. K. (1980) *Proc. Natl. Acad. Sci. U.S.A. 77*, 87−91.
21. Sebban, P., Robert, B., and Jolchine, G. (1985) *Photochem. Photobiol. 42*, 573−578.
22. Picorel, R., and Gingras, G. (1988) *Biochem. Cell Biol. 66*, 442−448.
23. Bolt, J., and Sauer, K. (1979) *Biochim. Biophys. Acta 546*, 54−63.
24. Davidson, E., and Cogdell, R. J. (1981) *Biochim. Biophys. Acta 635*, 295−303.
25. Davidson, E., and Cogdell, R. J. (1981) *FEBS Lett. 132*, 81−84.
26. Limantara, L., Koyama, Y., Katheder, I., and Scheer, H. (1994) *Chem. Phys. Lett. 227*, 617−622.
27. Bose, S. K. (1963) in *Bacterial Photosynthesis* (Gest, H., San Pietro, A., and Vernon, L. F., Eds.) pp 501−510, Antioch Press, Yellow Springs, Ohio.
28. Feher, G., and Okamura, M. Y. (1978) in *The Photosynthetic Bacteria* (Clayton, R. K., and Sistrom, W. R., Eds.) pp 349−396, Plenum Press, New York.
29. Laemmli, U. K. (1970) *Nature 227*, 680−685.
30. Nishizawa, E., Hashimoto, H., and Koyama, Y. (1991) *Chem. Phys. Lett. 181*, 387−390.
31. Yamaguchi, S., and Hamaguchi, H. (1995) *Appl. Spectrosc. 49*, 1513−1515.
32. Clayton, R. K. (1963) in *Bacterial Photosynthesis* (Gest, H., San Pietro, A., and Vernon, L. F., Eds.) pp 495−500, Antioch Press, Yellow Springs, Ohio.
33. Theiler, R., Suter, F., Zuber, H., and Cogdell, R. J. (1984) *FEBS Lett. 175*, 231−237.
34. Theiler, R., Suter, F., Wiemken, V., and Zuber, H. (1984) *Hoppe-Seyler's Z. Physiol. Chem. 365*, 703−719.
35. Williams, J. C., Steiner, L. A., and Feher, G. (1986) *Proteins 1*, 312−325.
36. Williams, J. C., Steiner, L. A., Ogden, R. C., Simon, M. I., and Feher, G. (1983) *Proc. Natl. Acad. Sci. U.S.A. 80*, 6505−6509.
37. Williams, J. C., Steiner, L. A., Feher, G., and Simon, M. I. (1984) *Proc. Natl. Acad. Sci. U.S.A. 81*, 7303−7307.
38. Cotton, T. M., and van Duyne, R. P. (1981) *J. Am. Chem. Soc. 103*, 6020−6026.
39. Callahan, P. M., and Cotton, T. M. (1987) *J. Am. Chem. Soc. 109*, 7001−7007.
40. Nishizawa, E., Limantara, L., Nanjou, N., Nagae, H., Kakuno, T., and Koyama, Y. (1994) *Photochem. Photobiol. 59*, 229−236.
41. Lutz, M. (1984) in *Advances in Infrared and Raman Spectroscopy* (Clark, R. J. H., and Hester, R. E., Eds.) Vol. 11, pp 211−300, John Wiley & Sons, New York.
42. Robert, B., and Lutz, M. (1985) *Biochim. Biophys. Acta 807*, 10−23.
43. Misono, Y., Limantara, L., Koyama, Y., and Itoh, K. (1996) *J. Phys. Chem. 100*, 2422−2429.
44. Holten, D., Hoganson, C., Windsor, M. W., Schenck, C. C., Parson, W. W., Migus, A., Fork, R. L., and Shank, C. V. (1980) *Biochim. Biophys. Acta 592*, 461−477.
45. Martin, J.-L., Breton, J., Hoff, A. J., Migus, A., and Antonetti, A. (1986) *Proc. Natl. Acad. Sci. U.S.A. 83*, 957−961.
46. Zinth, W., and Kaiser, W. (1993) in *The Photosynthetic Reaction Center* (Deisenhofer, J., and Norris, J. R., Eds.) Vol. II, pp 71−88, Academic Press, New York.
47. Connolly, J. S., Samuel, E. B., and Janzen, A. F. (1982) *Photochem. Photobiol. 36*, 565−574.
48. Ganago, A. O., Parker, E. P., Laible, P. D., Albrecht, A. C., and Owens, T. G. (1995) *Laser Phys. 5*, 693−698.

49. Lubitz, W. (1991) in *Chlorophylls* (Scheer, H., Ed.) pp 903−944, CRC Press, Boca Raton, FL.
50. Lendzian, F., Huber, M., Isaacson, R. A., Endeward, B., Plato, M., Bönigk, B., Möbius, K., Lubitz, W., and Feher, G. (1993) *Biochim. Biophys. Acta 1183*, 139−160.
51. Huber, M., Isaacson, R. A., Abresch, E. C., Gaul, D., Schenck, C. C., and Feher, G. (1996) *Biochim. Biophys. Acta 1273*, 108−128.
52. Tang, J., Dikshit, S. N., and Norris, J. R. (1995) *J. Chem. Phys. 103*, 2873−2881.
53. Straley, S. C., Parson, W. W., Mauzerall, D. C., and Clayton, R. K. (1973) *Biochim. Biophys. Acta 305*, 597−609.
54. Hayashi, H., Hamaguchi, H., and Tasumi, M. (1983) *Chem. Lett.*, 1857−1860.
55. Sturgis, J. N., Jirsakova, V., Reiss-Husson, F., Cogdell, R. J., and Robert, B. (1995) *Biochemistry 34*, 517−523.
56. Sturgis, J. N., Olsen, J. D., Robert, B., and Hunter, C. N. (1997) *Biochemistry 36*, 2772−2778.
57. Takiff, L., and Boxer, S. G. (1988) *J. Am. Chem. Soc. 110*, 4425−4426.
58. Stiel, H., Leupold, D., Teuchner, K., Nowak, F., Scheer, H., and Cogdell, R. J. (1997) *Chem. Phys. Lett. 276*, 62−69.
59. Petke, J. D., Maggiora, G. M., Shipman, L. L., and Christoffersen, R. E. (1980) *Photochem. Photobiol. 32*, 399−414.
60. Ohmine, I., and Karplus, M. (1978) *J. Chem. Phys. 68*, 2298−2318.
61. Zhang, J.-P., Chen, C.-H., Koyama, Y., and Nagae, H. (1998) *J. Phys. Chem. B 102*, 1632−1640.
62. Monger, T. G., Cogdell, R. J., and Parson, W. W. (1976) *Biochim. Biophys. Acta 449*, 136−153.
63. Monger, T. G., and Parson, W. W. (1977) *Biochim. Biophys. Acta 460*, 393−407.
64. Nuijs, A. M., van Grondelle, R., Joppe, H. L. P., van Bochove, A. C., and Duysens, L. N. M. (1985) *Biochim. Biophys. Acta 810*, 94−105.
65. Kingma, H., van Grondelle, R., and Duysens, L. N. M. (1985) *Biochim. Biophys. Acta 808*, 363−382.
66. Kingma, H., van Grondelle, R., and Duysens, L. N. M. (1985) *Biochim. Biophys. Acta 808*, 383−399.
67. Campillo, A. J., Hyer, R. C., Monger, T. G., Parson, W. W., and Shapiro, S. L. (1977) *Proc. Natl. Acad. Sci. U.S.A. 74*, 1997−2001.
68. van Grondelle, R. (1985) *Biochim. Biophys. Acta 811*, 147−195.
69. Bakker, J. G. C., van Grondelle, R., and den Hollander, W. T. F. (1983) *Biochim. Biophys. Acta 725*, 508−518.
70. Bradforth, S. E., Jimenez, R., van Mourik, F., van Grondelle, R., and Fleming, G. R. (1995) *J. Phys. Chem. 99*, 16179−16191.
71. Gomez, I., Sieiro, C., Ramirez, J. M., Gomez-Amores, S., and del-Campo, F. F. (1982) *FEBS Lett. 144*, 117−120.
72. Picorel, R., Lefebvre, S., and Gingras, G. (1984) *Eur. J. Biochem. 142*, 305−311.
73. Gomez, I., Sanchez, A., and del Campo, F. F. (1985) *Physiol. Veg. 23*, 583−591.
74. Gingras, G., and Picorel, R. (1990) *Proc. Natl. Acad. Sci. U.S.A. 87*, 3405−3409.
75. Norris, J. R., Dikshit, S. N., Popov, M., Weber, S., Tiede, D., Tang, J., Hanson, D. K., and Schiffer, M. (1996) in *Symposium on Electron Transfer in Proteins and Supermolecular Assemblies at Interfaces*, Hayama, Japan.

BI981803Q